AEROSOL BEHAVIOR IN HIGH PRESSURE ENVIRONMENTS

Robert A. Gussman, et al

Bolt Beranek and Newman, Incorporated
Cambridge, Massachusetts

31 October 1969

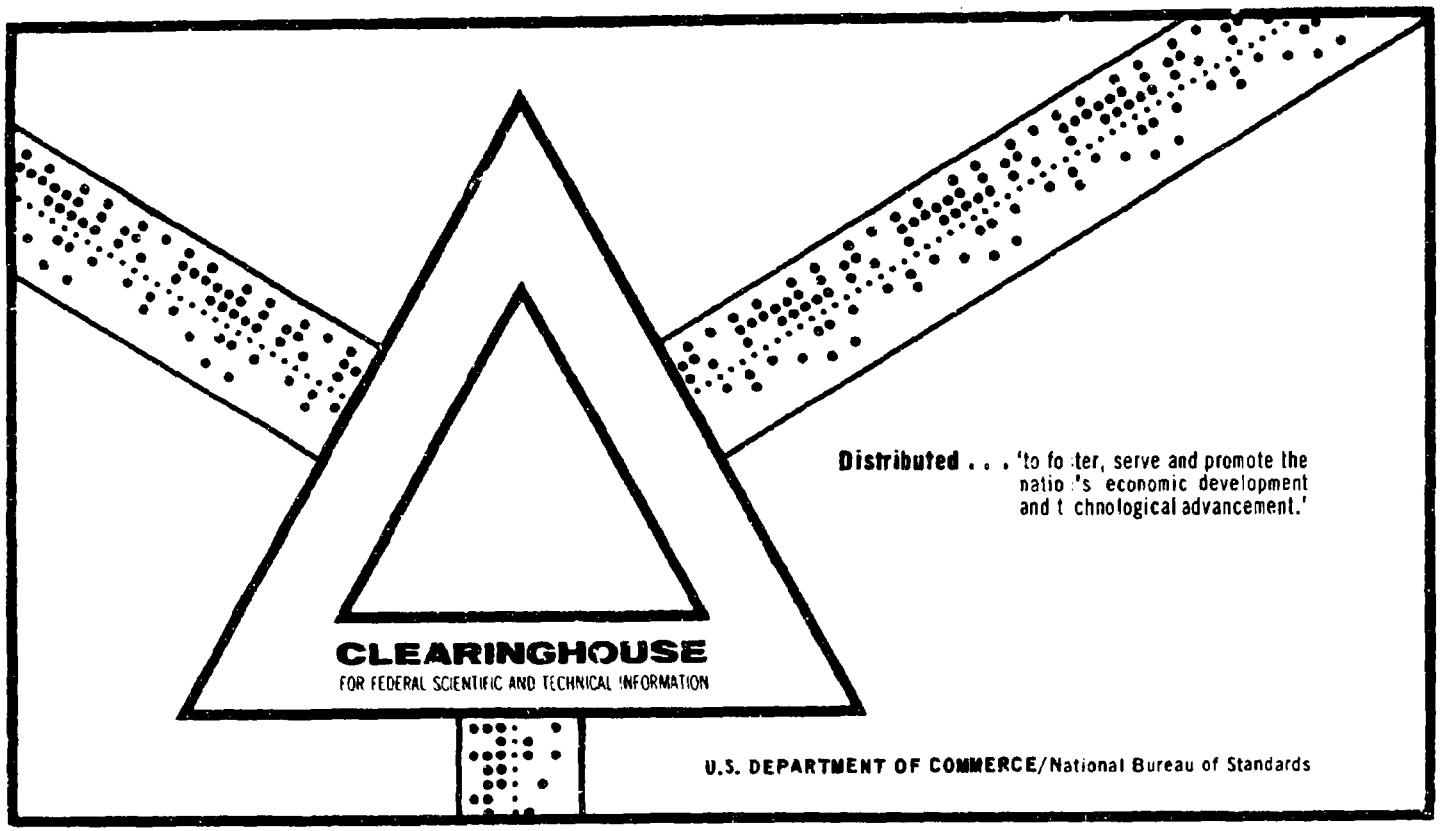

BOLT BERANEK AND NEWMAN INC

CONSULTING · DEVELOPMENT · RESEARCH

Report No. 1884

31 October 1969

AEROSOL BEHAVIOR IN HIGH PRESSURE ENVIRONMENTS -- Special Report

by: Robert A. Gussman
Anthony M. Sacco

Sponsored by:

Department of the Navy
Office of Naval Research
Washington, D.C. 20360

Contract No. N00014-69-C-0228
NR 303-829

Report No. 1884 31 October 1969

AEROSOL BEHAVIOR IN HIGH PRESSURE ENVIRONMENTS -- Special Report

by: Robert A. Gussman
Anthony M. Sacco

Sponsored by:

Department of the Navy
Office of Naval Research
Washington, D.C. 20360

Contract No. N00014-69-C-0228
NR 303-829

LIST OF ILLUSTRATIONS

LIST OF ILLUSTRATIONS - con't.

LIST OF TABLES

Section 1: INTRODUCTION

The specific purpose of this special report is to present our final results of work carried out on two related subjects. Namely, an experimental study of the evolution of particles from resistant heating elements in high pressure environments and secondly, computations based on a pulmonary deposition model for high pressure environments. Initial progress in both areas was presented in our recent interim report (Rept. No. 1845, dated 31 July 1969). All of the experimental and theoretical work on these two subjects has been completed and we feel it necessary in the interests of the project to present our final results separately rather than at the conclusion of this year's effort.

This report incorporates a. of the introductory material presented in our interim report and is intended to be complete without the necessity for referencing the previous document.

Section 2: EXPERIMENTAL DETERMINATIONS OF THE PRODUCTION OF AEROSOLS FROM HEATED SURFACES IN HELIUM-OXYGEN ATMOSPHERES AT VARIOUS PRESSURES.

The purpose of this series of experiments was to determine how the size distribution and number concentration of aerosols produced by heating elements vary with pressure in our helium-oxygen environment. Because resistance heating is a technique used in deep-submersible vessels (where smoking is virtually impossible), heating and cooking activities seem to be the main identifiable sources of aerosols arising within such environments. Discussions of the production of particles from nichrome, tungsten, and other resistance heating elements are numerous. The more recent observations are typified by Refs. 1, 2, 3 and 4. Generally, the literature presents data on the particle size distributions and number concentrations obtained from various wires that have been brought to a red heat under stable flow conditions. Electron microscopy is the most common technique for the analysis of solid submicron aerosol samples. Occasionally, new information has been obtained such as that pointed out by Goldsmith et al., [4] who performed a chemical analysis of the particles produced from a heated nichrome wire. They determined that the composition of the aerosol was almost entirely chromium - a marked contrast to the initial composition, which was 80% nickel and 20% chromium. The process by which aerosols are formed in the vicinity of a heated wire is apparently simple; molecules boil off the surface of the wire in great numbers, and upon entering into the cooler air surrounding the wire, they condense from the vapor phase and agglomerate into particles in the submicron size range (in air at ambient pressure). When one considers the decrease in oxygen with the increase of depth [5] and takes into account the high heat transfer rate in helium, it seems logical that the number concentrations and particle dimensions produced in deep-submersible vessels will

vary from those produced in air at ambient pressure. Further, since our initial studies[5] have indicated relatively greater lower pulmonary deposition for submicron aerosol particles, it is of prime importance to correlate thermal measurement data on aerosol generation with postulated pulmonary deposition.

2.1 Experimental Apparatus

The test chamber designed for both the generation and the thermal deposition of aerosols from a hot wire is shown in Figures 1 and 2. The removable cap contains a pair of electrodes across which wires up to 1 mm in diameter can be stretched. Two fixed wire heights above the deposition surface may be used, either 0.300 or 0.185 inches. The deposition surface is a glass microscope cover slip 18 mm in diameter by 0.25 mm thick. During tests and for purposes of convenient transport and handling, these glass disks are contained in the stainless steel cassettes (Figure 3). The proximity of the hot wire to a thin glass collection surface, resting on a massive steel base, at ambient temperature, allows both generation and thermal deposition to be accomplished in one continuous operation. A simple trunnion, yoke, and screw arrangement secure the cover to the test chamber; this arrangement has proven leak-proof for pressures up to 600 psia. The collected sample, with its cassette, is transported on a carrying rack (Figure 3), which is covered with a glass dome that is clamped into position. Each rack holds six samples.

Samples for normal electron microscopy are collected on 3 mm diameter 100-mesh carbon-coated grids, which are simply placed on top of the stainless steel cassette. The upper ring and glass sample disk are omitted. These samples may then be transported in readily available commercial containers designed for the purpose.

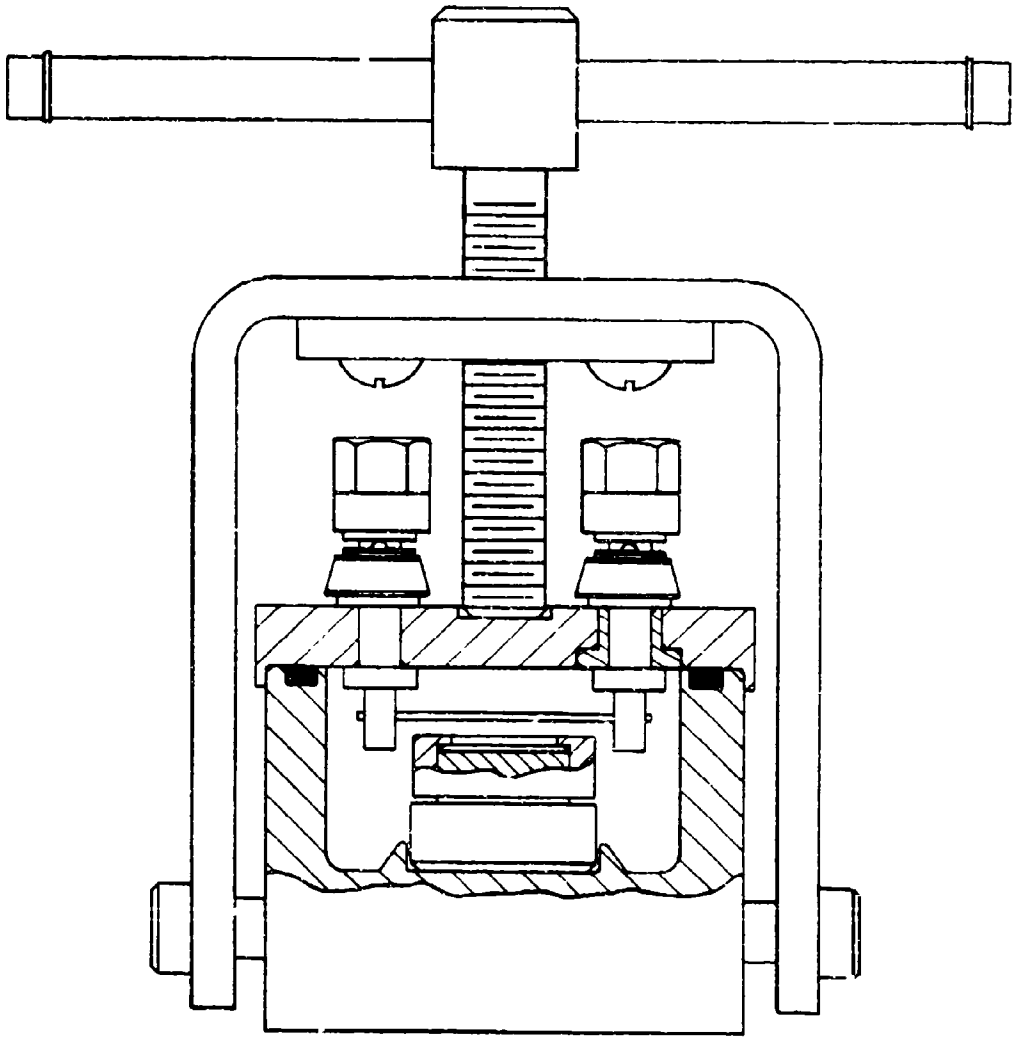

Figure 1. Sectional View of Aerosol Test Vessel

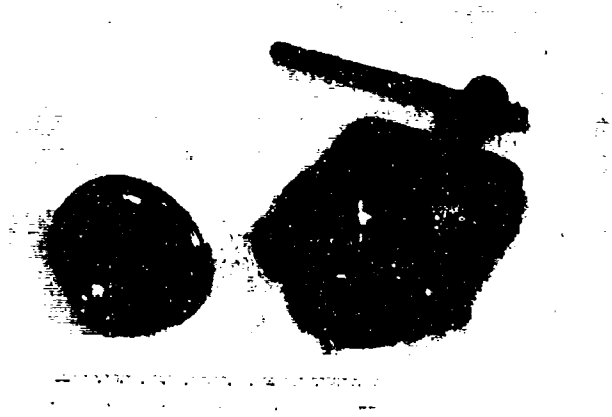

Figure 2. Aerosol Test Vessel - Disassembled

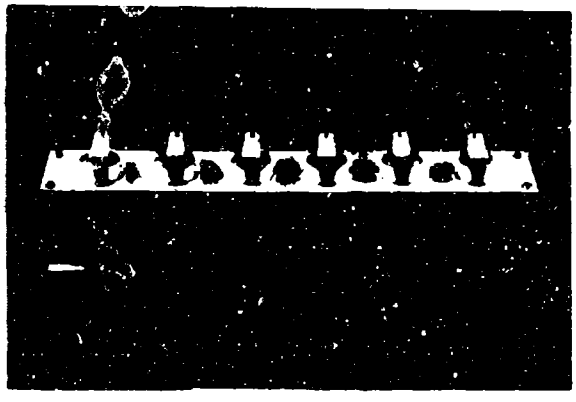

Figure 3A. Cassette Rack

Figure 3B. Cassette - Disassembled

The standard gas mixture for all tests, regardless of total pressure, consists of 160 mm Hg PO_2 plus helium. The apparatus used for achieving the proper mixture over the desired total pressure range of 10 to 500 psia is shown in Figure 4 and 6. The equipment consists of a high quality pressure gauge, a vacuum gauge, a two-stage vacuum pump capable of pumping down to 1 micron Hg pressure, and suitable valving. All gas pumped into or out of the test vessel is filtered through a 25 mm disk of Millipore VF. The operating routine is discussed below under experimental procedure.

Electrical energy for heating the wires is supplied from an 18V dc battery controlled by the apparatus shown in Figures 5 and 6. The equipment consists of a 25V dc meter and a 25 amp meter. Both meters have been calibrated. A rheostat varies the voltage applied to the wire and a push-button switch permits precise control of current flow duration.

Because of the fineness of the particles under investigation, the requirement for the prevention of contamination from atmospheric dust is critical. Accordingly, a small "clean area" has been constructed within which experiments and sample-taking operations are performed. The area, shown in Figure 7 encompasses a 2 ft x 2 ft pleated fiberglass filter of the high-efficiency type fitted with appropriate plenums and a 400 cfm capacity fan. The inside of the working area is completely lined with formica. A side discharge, suction source, 4 in. dia., is placed close to the face of the filter, to remove fumes resulting from preliminary solvent cleaning operations.

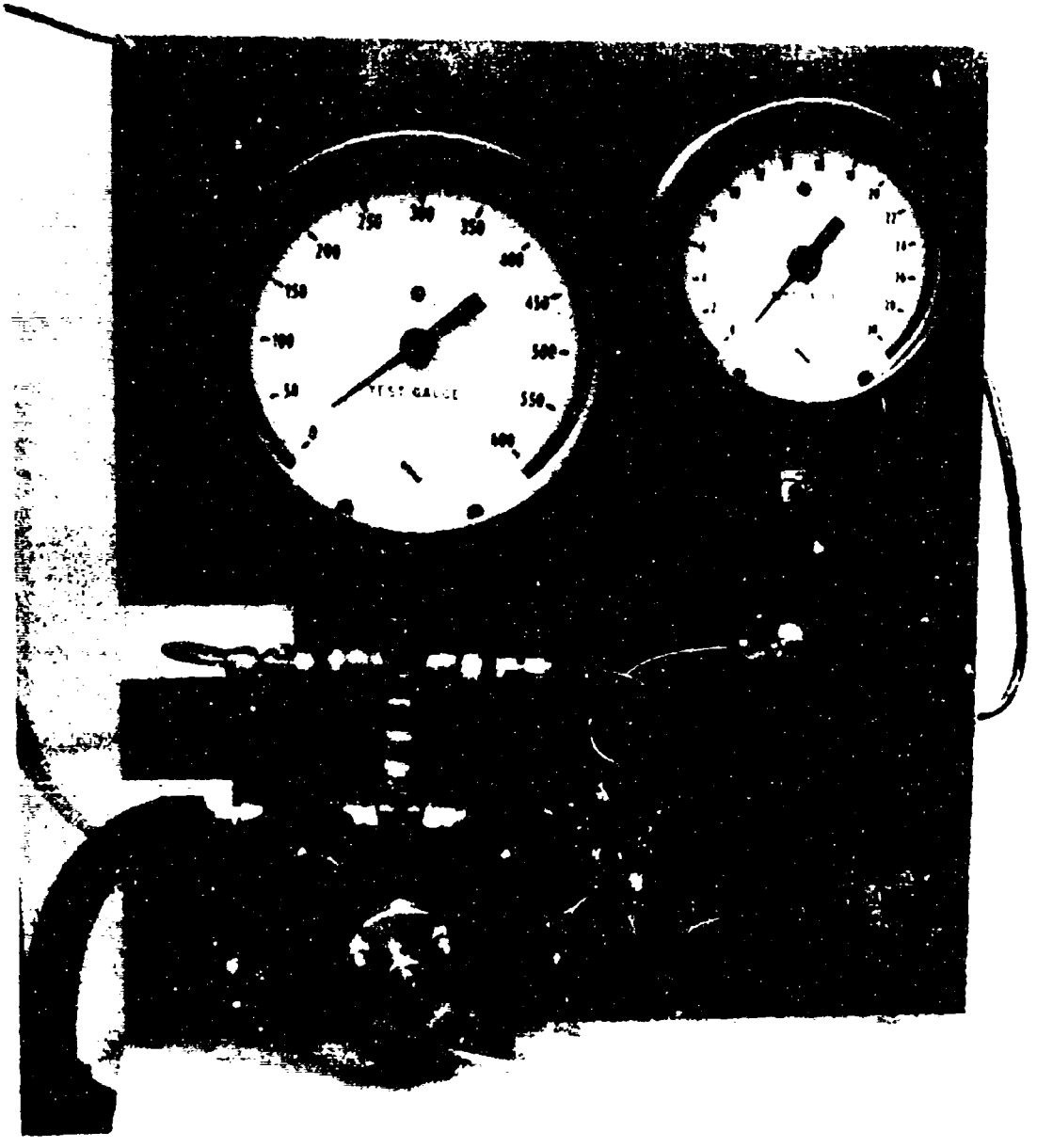

Figure 4. Gas Mixing Control Panel

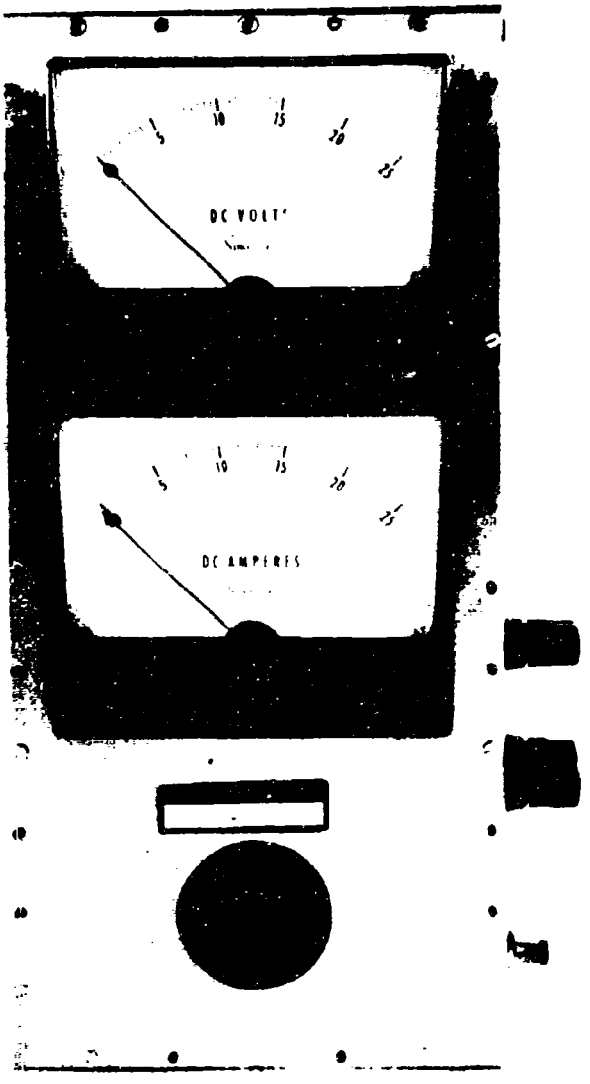

Figure 5. Electrical Controls for Hot Wire

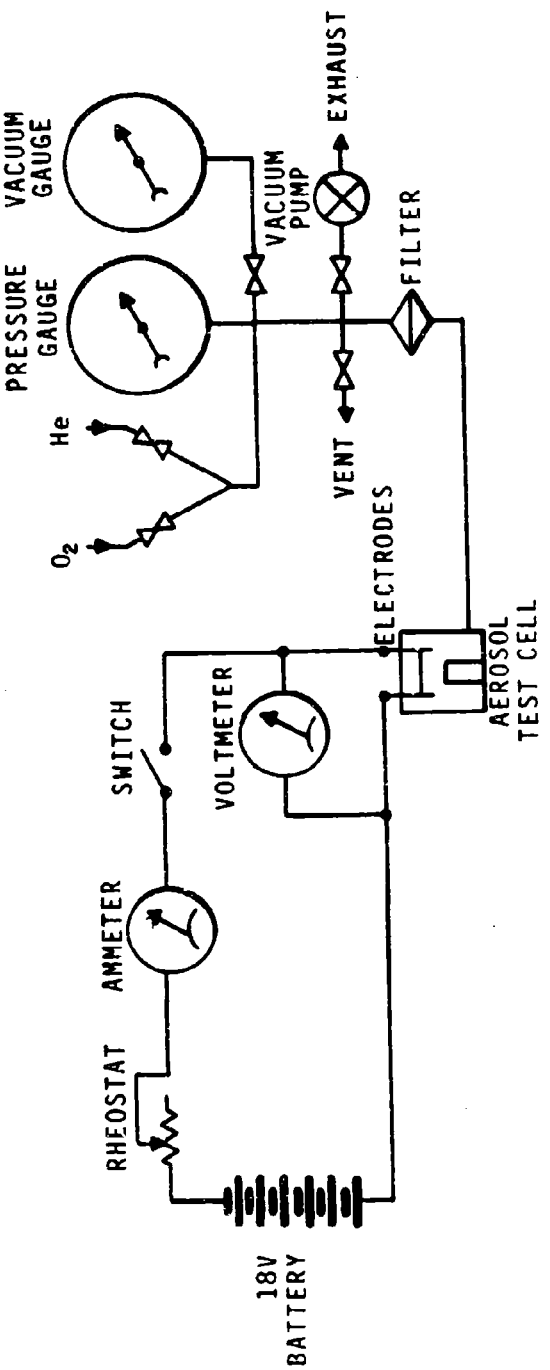

Figure 6. Schematic Diagram of Aerosol Generation and Sampling Apparatus

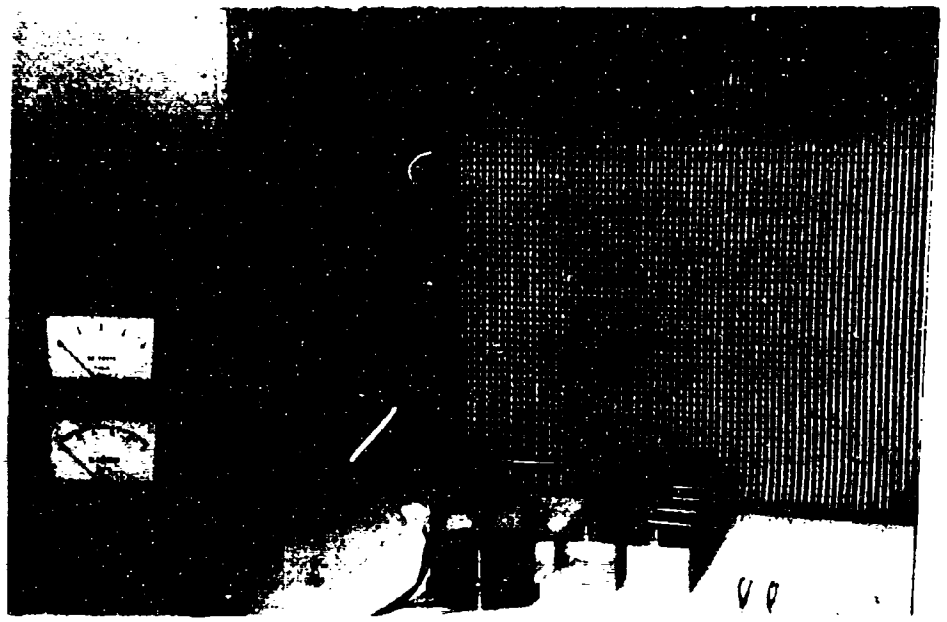

Figure 7. Clean Area and Test Apparatus

2.2 Experimental Procedure

All parts of the experimental apparatus are first placed within the "clean area" and thoroughly rinsed with a high-purity final-filtered fluorocarbon solvent. A pre-cut length of nichrome wire is fastened to the binding posts; the bomb is sealed, evacuated, and filled with high purity helium to a pressure of 15 psia. The wire is then heated by impressing 3V across it (8.8 amps for a 0.020 in. diameter wire) for 0.2 minutes. The purpose of this procedure is to burn off any impurities that may be on the surface of the wire. A glass side is selected, cleaned, and placed in its steel cassette; the cassette is placed in the test chamber, which is resealed. The test chamber is evacuated to approximately 1 micron Hg pressure followed by a re-pressurization with pure oxygen to 160 mm Hg. Helium is then admitted to the desired test pressure. The discharge of particles from the test wire is accomplished by impressing upon the wire a pre-selected voltage for a fixed period of time. The over-pressure is then released from the test chamber; the chamber is opened; and the cassette is removed from the chamber and placed in its transport rack. The procedure may then be repeated.

Sample analysis is performed either by scanning electron microscopy of the untreated slide or by direct electron microscopy of carbon coated, nickel grids.

2.3 Initial Range Finding Tests

In order to make a series of tests at various pressures comparable, it was necessary to establish a constant quantity of energy to be pulsed through a wire of fixed dimension for each series. The quantity of energy, expressed in watt seconds, is given by the simple formula:

$$\text{Energy} = EIt \qquad (1)$$

where: E = voltage - volts

I = current - amps

t = time - seconds

It was also necessary to maintain the wire temperature constant at each pressure level. Since thermal conductivity is different for helium-oxygen mixtures than for air and is also different at various pressures, we measured wire temperature at each pressure. We fabricated a chromel-alumel thermocouple from 0.001 in. dia. wire and welded it directly to the center of a sample 0.020 in. nichrome wire. Special binding posts were fitted to a cap for these tests. Observations in air indicated that the very low mass of the thermocouple caused no dead spot along the wire. When this apparatus was inserted into the bomb, a series of voltage, current, and temperature measurements was made at each of the pressures (10 to 500 psia) used on this project. The results are shown in Figure 8 and 9.

To insure a usable production of particles, we selected a high red heat corresponding to 2200^{o}F as the operating temperature for later tests. By reading horizontally across the 2200^{o}F line in Figure 9, one may determine the power required at each pressure for maintaining wire temperature constant. Then, having selected a fixed quantity of energy at the lowest pressure, one may use the above equation to calculate the operating time (current duration). Similarly, maintaining this total energy quantity, one may calculate the individual operating time for other pressures. The determined energy quantity to maintain a 2200^{o}F wire temperature and yield reasonable operating times (approximately 1 minute) was 1160 watt-secs. The

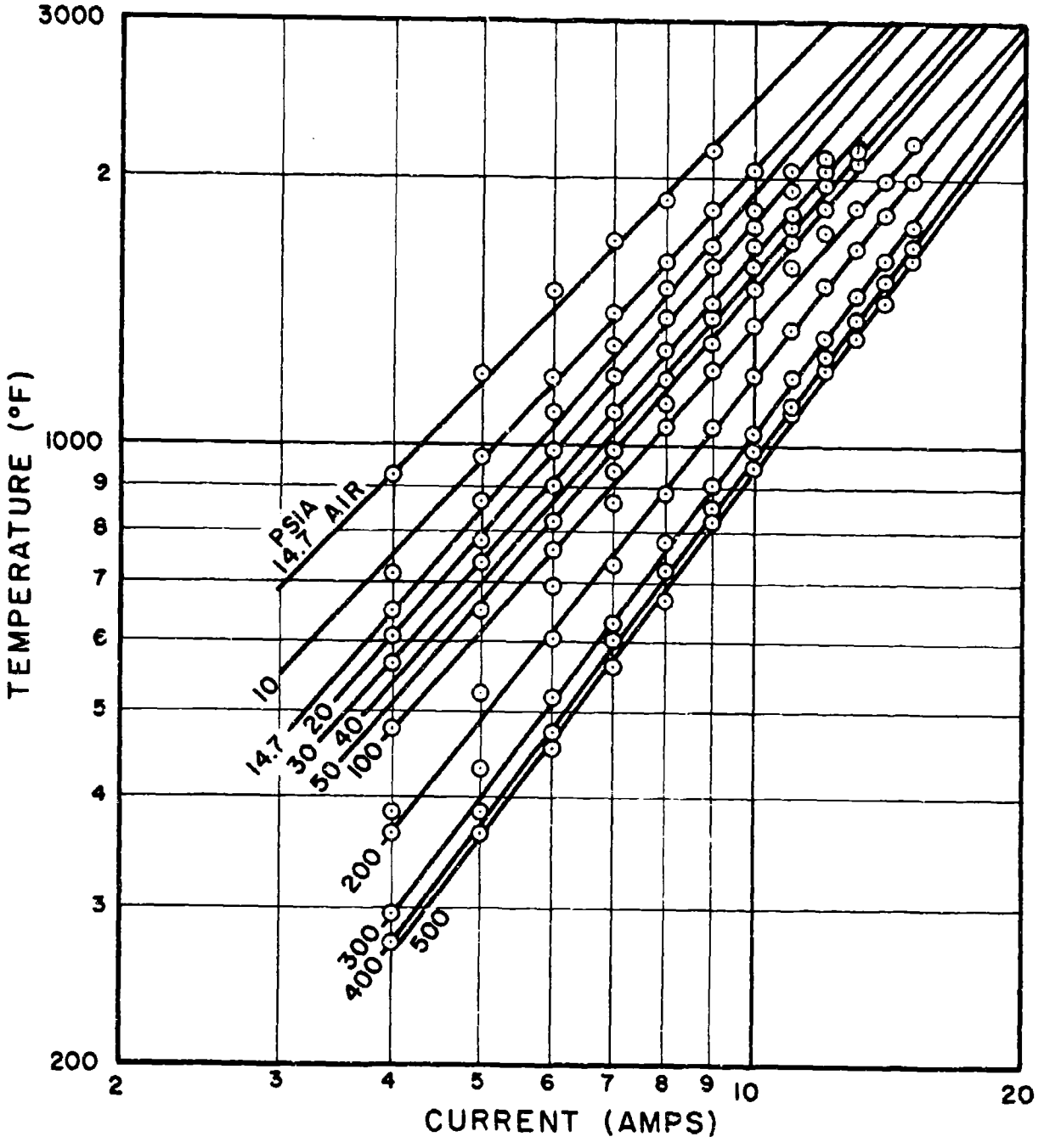

Figure 8. Temperature vs Current. 0.020 inch Nichrome Wire (1-5/16 in. long) Heated in He-O_2 (PO_2 = 160 mm Hg) at Various Pressures.

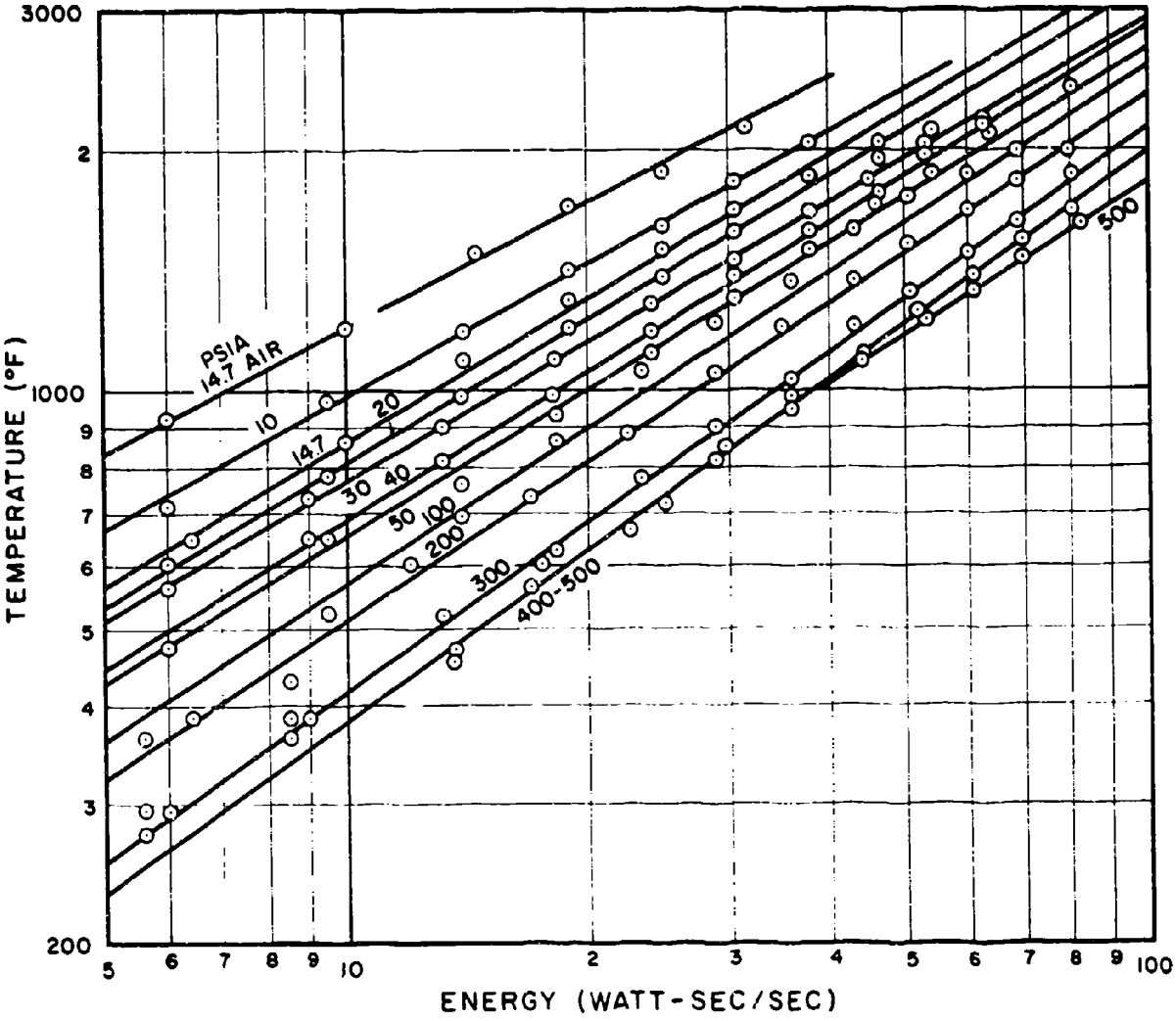

Figure 9. Temperature vs Energy Per Unit Time. 0.020 inch Nichrome Wire (1-5/16 in. long) Heated in He-O_2 (PO_2 = 160 mm Hg) at Various Pressures.

parameters for each test are shown in Table 1. Experimental difficulties were later encountered at the high pressure conditions, above 100 psia, wherein too few particles were being generated for analytical purposes. In these cases (and subsequently discussed under Results) the energy was either doubled or tripled simply by adjusting the operating time. Also, it was determined necessary to run tests at 10 psia intervals between 50 and 100 psia and the necessary current voltage relationships were determined by extrapolating the curves in Figures 8 and 9.

2.4 Results

For the initial series, we used a variety of operating times and pressures as well as two heights of the wire above the stage. The wire diameter was fixed for all tests at 0.020 in. (1/2 mm), and the length at 1-5/16 in. Test conditions for this first series of experiments are summarized in Table 2. These tests were run before temperature calibration was accomplished. Representative scanning electron photomicrographs, shown in Figure 10, correspond to the samples taken on tests #11 and 12, which at that time were expected to yield the highest concentrations. The blurred appearance of the particles in the photographs is not caused by deficiencies in technique but rather by the fact that the particles are below the limits of resolution for scanning electron microscopy. An approximate sizing from these photographs indicates that the particles vary from 0.02 to 0.1 microns. Because of the expense involved in performing these types of analysis, the other samples taken were not evaluated.

Table 1. Operating Parameters for Nichrome Wire at 2200°F in a He-O_2 Gas Mixture (PO_2 = 160 mm Hg)*

Pressure psia	Current Amps-I	Power Watts-IE	Energy Watt-Second IEt	Duration Seconds
10	10.6	42.7	1160	27.2
14.7	11.2	47.8	1160	24.3
20	11.8	53.0	1160	21.9
30	12.8	61.0	1160	19.02
40	13.4	64.9	1160	17.89
50	13.8	71.0	1160	16.34
100	15.0	78.5	1160	14.8
200	16.1	89.5	1160	12.98
300	17.4	103.0	1160	12.7
400	17.7	116.0	1160	10.0
500	18.8	133.0	1160	8.72
14.7 (air)	9.5	31.5	1160	36.9

*wire diameter = 0.020 in., L = 1-5/16 in.

Table 2. Aerosols Generated from Ni-Cr Wire* - Initial Range Finding Tests - Glass Substrate.

Test No.	Pressure** psia	Voltage E	Current A	Time Min.	Energy Watt-Seconds	Position*** Hi-Low
1	14.7	3	8.6	0.5	774	Low
2	14.7	3	8.9	0.5	800	Hi
3	Air	3	8.7	0.5	783	Low
4	Air	3	8.8	0.5	792	Hi
5	50	3	8.7	0.5	783	Low
6	50	3	8.9	0.5	800	Hi
7	500	3	8.7	0.5	783	Low
8	500	3	8.9	0.5	800	Hi
9	50	3	8.8	3.0	1582	Hi
10	50	4	11.8	0.5	1415	Hi
11	50	4	11.7	0.5	1405	Low
12	50	5.2	15	0.5	2340	Low

*-High purity wire 0.02 in. diameter.

**-He + 160 mm Hg PO_2 = total pressure. "Air" indicates filtered room air at 14.7 psia.

***-High-wire is 0.3 in. above sample collecting surface. Low-wire is 0.185 in. above sample collecting surface.

Test No. 11

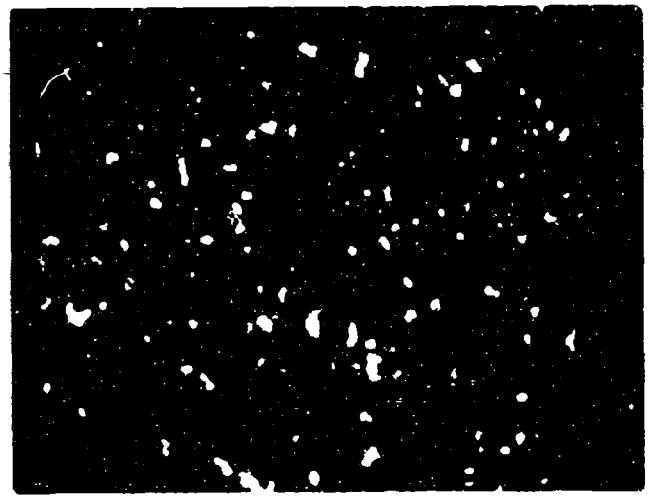

Test No. 12

Figure 10. Scanning Electron Photomicrographs of Aerosol Collected from Heated Nichrome Wire - (1 cm = 0.2μ)

At this point, a long series of tests were run in which all of the samples were taken on carbon-coated nickel, electron microscope grids. All analyses were accomplished by electron microscopy of the untreated samples. Representative electron photomicrographs are shown in Figures 11a and 11b. Early in this series it was found that there was no necessity of the higher (0.3 in.) generating wire position and it was eliminated. All results have been accumulated and are shown with the operating parameters in Table 3. Many of the grids examined contained no sample whatsoever. At pressures below 100 psi this was eventually found to be due to the low quality of grids initially utilized which were made up at a local laboratory. This problem was rectified by the purchase of commercially available grids.* Suspecting that a different factor was causing the problem, additional tests were run at 60, 70, 80, and 90 psia. It may also be noted in Table 3 that the planned energy level of 1160 watt-secs per test was abandoned for pressures above 100 psia and multiples of two or three times the planned figure were utilized. The reason for this change was that analysis of the early photomicrographs at the lower pressures revealed a rapidly decreasing numbers concentration with increasing pressure. Since temperature is a constant we adopted the trial postulation that numbers concentration is directly related to the quantity of energy applied. Therefore, the two or three times increment was adopted in order to obtain a sufficient number of particles for analysis.

Particles were sized by using an over-lay grid on 8" x 10" photomicrographs. The grid consisted of a series of lines made up as a transparency. The distance

*Ladd Research, Burlington, Vermont, Catalog no. 251.

Pressure = 10 psia Magnification = 80,000X

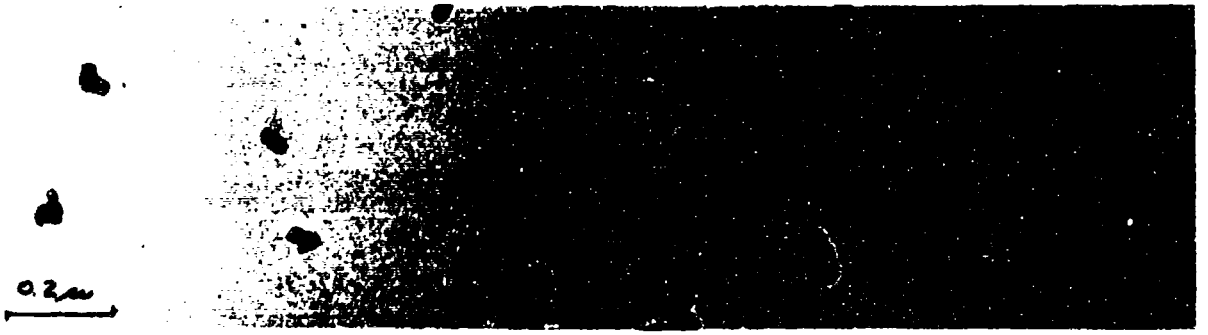

Pressure = 50 psia Magnification = 80,000X

Pressure = 100 psia Magnification = 70,000X

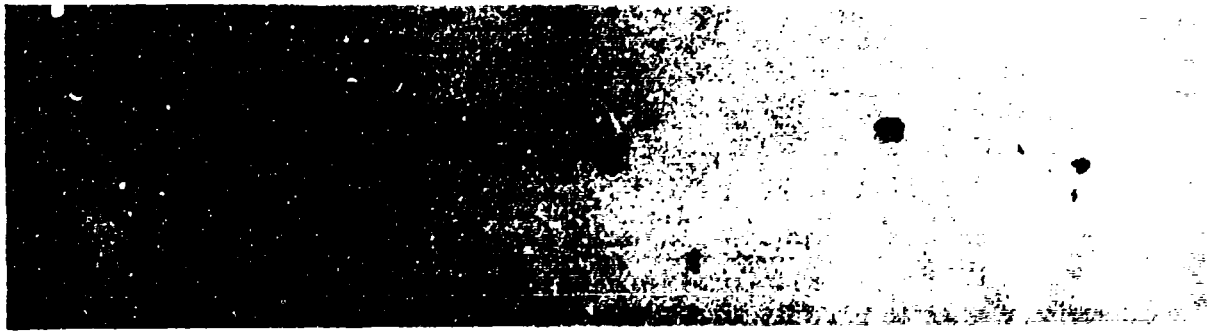

Pressure = 200 psia Magnification = 75,500X

Figure 11a. Electron Photomicrographs of Particles Thermally Precipitated from a Heated Nichrome Wire in an He-O_2 Atmosphere. -- Pressures and Magnifications as noted.

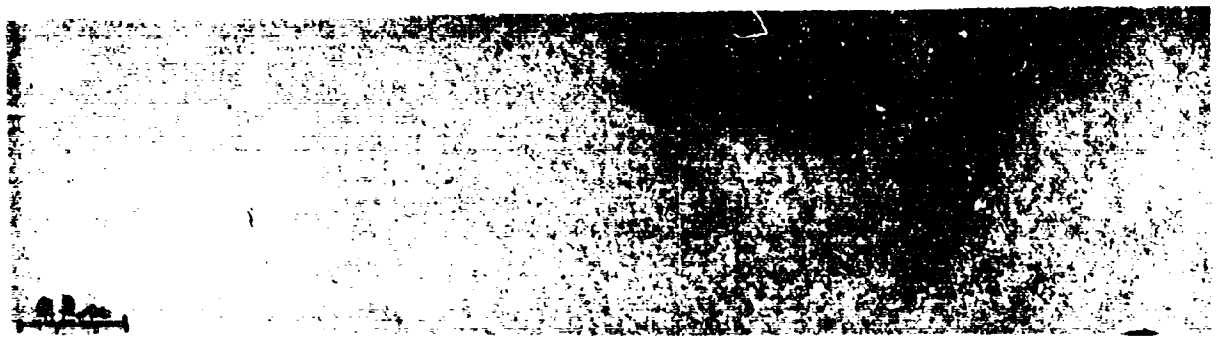

Pressure = 300 psia Magnification = 75,000X

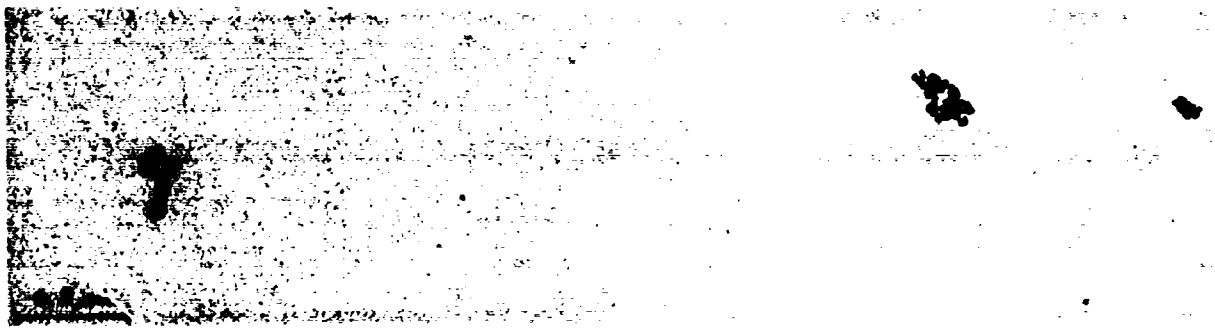

Pressure = 400 psia Magnification = 80,000X

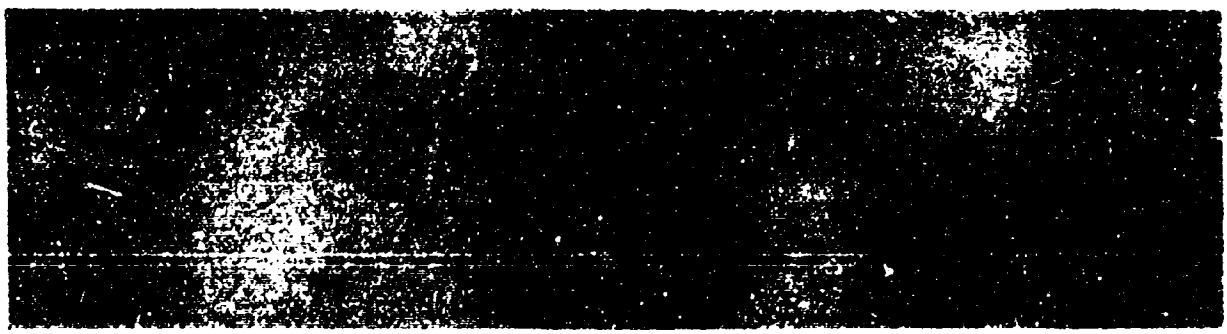

Pressure = 500 psia Magnification = 75,500X

Pressure = 14.7 psia (air) Magnification = 80,000X

Figure 11b. Electron Photomicrographs of Particles Thermally Precipitated from a Heated Nichrome Wire in an He-O_2 Atmosphere. -- Pressures and Magnifications as noted.

Table 3. Aerosols Generated from Ni-Cr Wire* - Carbon on Nickel Substrate.

Pressure** psia	Voltage E	Current A	Time Min	Energy watt-seconds	Count Median Diameter	Mass Median Diameter	Psuedo Standard Deviation $\sigma_{g(i)}$
10	10.6	3.8	0.453	1097	0.0134	0.104	2.27
14.7	11.2	4.0	0.404	1090	0.0160	0.084	2.10
20	11.8	4.2	0.365	1086	0.0205	0.115	2.13
30	12.8	4.6	0.317	1123	0.0183	0.120	2.20
40	13.4	4.9	0.298	1175	0.030	0.125	2.00
50	13.8	5.0	0.273	1130	0.035	0.099	1.81
60	14.1	5.1	0.269	1151	0.037	0.112	1.84
70	14.3	5.2	0.260	1160	0.0328	0.100	1.85
80	14.5	5.3	0.252	1161	0.0365	0.091	1.74
90	14.8	5.4	0.242	1161	0.0254	0.125	2.07
100	15.0	5.5	0.494	2450	0.0370	0.116	1.86
200	16.1	5.4	0.648	3380	0.0410	0.077	1.58
300	17.4	6.0	0.636	3990	0.102	0.280	1.78
400	17.7	6.3	0.501	3350	0.0463	0.150	1.87
500	18.8	6.5	0.438	3210	0.066	0.127	1.60
Air	3.6	9.5	1.232	2530	0.0435	0.111	1.75

*High purity wire 0.02 in. diameter.

**He + 160 mm Hg PO_2 = total pressure. "Air" indicates filtered room air @ 14.7 psia.

from the fiducial line increased as $\sqrt{2}$ in the manner of the well-known Porton graticule. The number of particles in each interval was tabulated by hand and the mass ($M_{g'}$) and count (M_g) median diameters were calculated according to the method recommended by Corn et al.[6] This technique does not force the distributions into a log normal mode and they were, in fact, found to be non-log normal. All calculations were accomplished on our Telcomp computer system by utilizing a short program written for the purpose. It should be noted in Table 3 that a column is labeled "pseudo standard deviation - $\sigma_{g(i)}$." This pseudo or imaginary number is a descriptor we have found useful for monitoring trend changes in non-log normal distributions. It is determined by taking the ratio of the count median and mass median diameters and back calculating what might be the geometric standard deviation via Hatch-Choate equations.[7] This number then ($\sigma_{g(i)}$) represents a measure of the distribution, assuming log normality, and is an indicator of the distribution under non-log normal conditions which is the current case without exception.

The determined values of the count median diameter (M_g) and the mass median diameter ($M_{g'}$) is plotted in Figure 12. While there is some scatter in the results, the trends are clear and the lines were determined by a least squares regression analysis. The count median diameter increases with increasing pressure according to the relationship:

$$M_g = 0.00574\ P^{0.4051} \qquad (2)$$

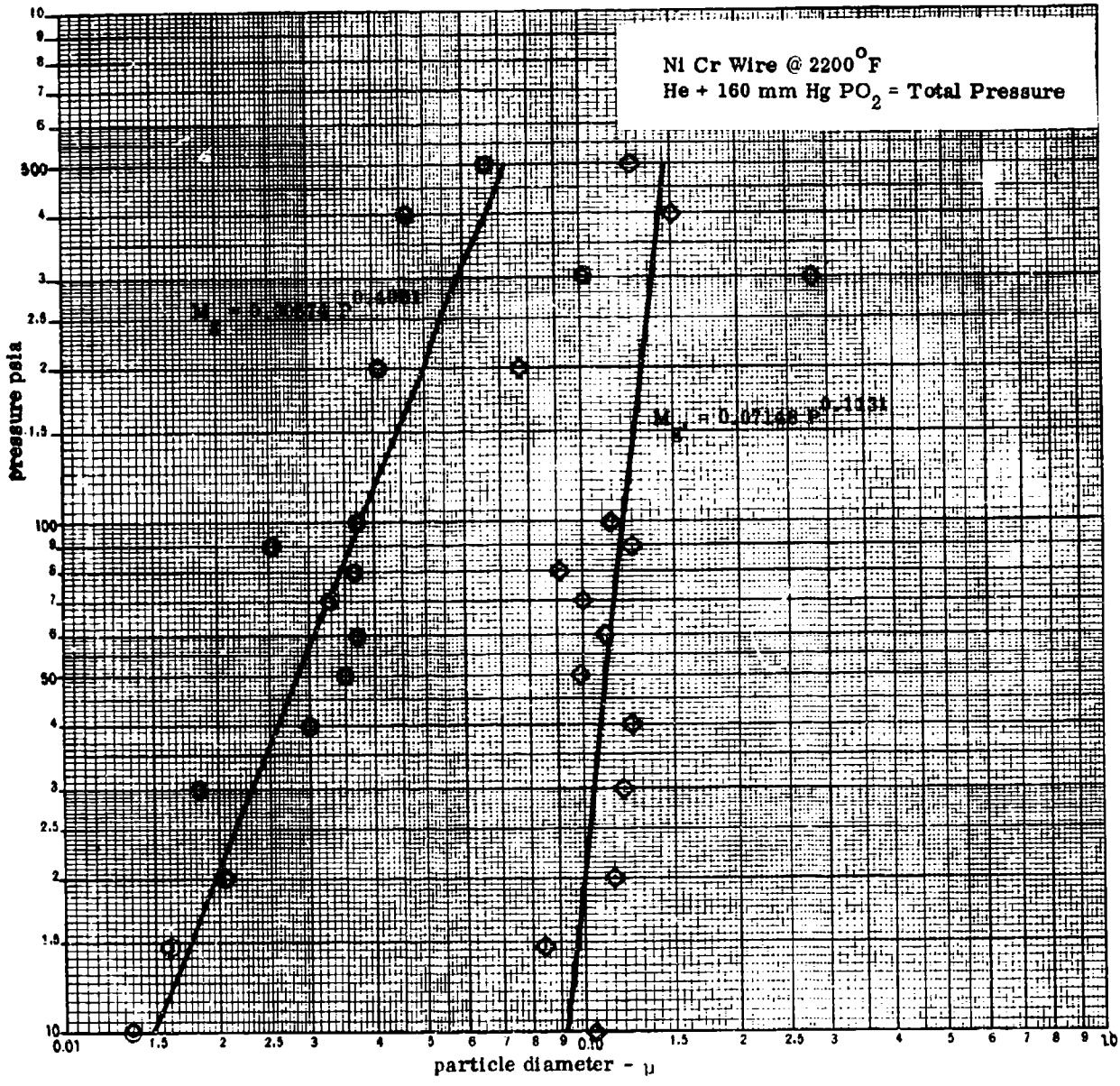

Figure 12. Count (M_g) and Mass ($M_{g'}$) Median Diameters vs Pressure.

The mass median diameter also increases with increasing pressure but in a much less rapid manner almost to the point of being negligible. The increase may be described by the relationship:

$$M_{g'} = 0.07148\ P^{0.1131} \tag{3}$$

Physically, the reasons for the differing slopes can be readily explained. Gross examination of the photomicrographs (Figures 11a and 11b) shows a reduction in the numbers of smaller particles as pressure increases. Further there is no readily observable appearance of very large particles, merely a reduction in the smaller ones. This conclusion is supported, mathematically, by the decreasing trend (with increasing pressure) of the values of $\sigma_{g(i)}$ (Table 3). This accounts for the convergence of the M_g and $M_{g'}$ curves shown in Figure 12.

A second notable feature, which is apparent from an examination of the photomicrographs in Figures 11a and 11b, is the marked reduction in the numbers of particles produced. In the performance of these experiments approximately five to seven photomicrographs of the grid area were examined per test. In all cases, every particle present was counted. At each pressure these counts were normalized to a common area expressed in square microns and further normalized to an energy level of 1160 watt-secs. Number of particles per square micron vs pressure has been plotted in Figure 13 and thereby yields a relative indication of numbers concentration vs pressure. The variation in concentration between 10 and 500 psia amounts to a reduction of approximately 500 times.

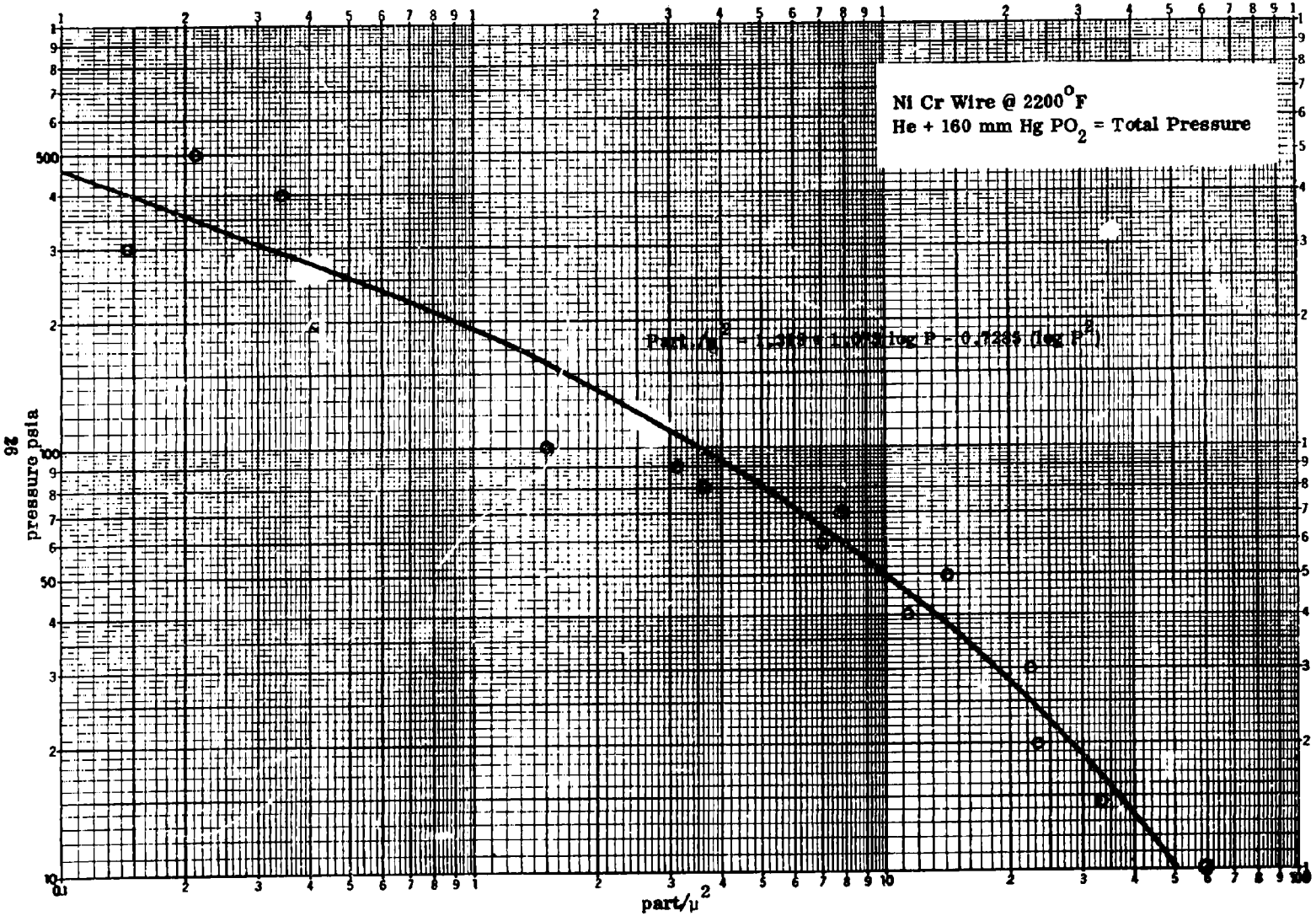

Figure 13. Particle Concentration vs Pressure.

2.5 Conclusions

Several useful conclusions may be drawn from the preceding results. However, it is first necessary to have a clear understanding of the limitations under which they are valid. Of all the possible sources of particulate within a deep submergence environment only one has been evaluated. The single source studied was for thermally generated metallic particles of high specific gravity in the submicron size range. Test limitations such as the stationary air mass into which particles are being generated, the use of a single pre-selected temperature, and a rigid generation-sampling configuration are all factors which limit the applicability and usefulness of possible conclusions. Nevertheless, all of the stated limitations were clearly understood and recognized prior to the inception of this experiment as being both practical and economical boundaries of the investigation.

(1) Under fixed energy and temperature conditions the median diameter of particles produced from a heated wire increases with increasing pressure. The count median diameter increases more rapidly than the mass median diameter and the nature of the increase is such that less of the finer particles are observed. This observed change may be due to the decreasing weight percentage of oxygen available as pressure increases but is more likely attributable to alterations in mobility, diffusivity, and high heat transfer rates with the increased quantity of helium (at increased pressure). Particles produced within our apparatus in air at ambient pressure do not directly relate to those produced in the $He-O_2$ environment as M_g (0.044μ) equals the $He-O_2$ results at 50 psia. $M_{g'}$ for air (0.111μ) corresponds to the $He-O_2$ size at 150 psia.

(2) The numbers concentration decreases remarkably with increased pressure. Gross investigation of the data indicates that there is not only a loss of smaller particles, possibly to the larger ones, but there also is a distinct reduction in the total number of particles generated, that is, a reduction in the total quantity of mass released from the wire. The number of particles/μ^2 produced in air (0.91) corresponds to the He-O_2 result at 200 psia.

(3) Based upon the preceding data and results it is possible to completely determine the parameters governing the generation of particles in terms of: size distribution and numbers concentration from hot wires. In order to do this three additional variables would have to be added to the study. One would be a variation in the oxygen content of the atmosphere; another would certainly be the result of a temperature variation and the third, would be air flow rate over the wire. This would entail a highly rigorous and intensive study which is not felt to be justified at this time. The results obtained tend towards more conservative rather than more radical potential exposures from this one source. Further, the presence of many trace contaminants in a real environment might dramatically alter the nature of particles generated from this source. The important variable of air flow over the wires will be subsequently investigated as part of a planned filtration experiment.

Section 3: PULMONARY DEPOSITION STUDIES

In the initial consideration of pulmonary deposition in high pressure environments,[5] an attempt was made to modify a deposition model by generalizing the equations governing the physical behavior of aerosols for the gas composition and pressures involved. Problems arose because the papers describing the several models considered[8,9,10,11,12,13,14] did not contain sufficient information to function them directly. The only exception was the paper concerning the earliest model by Findeisen.[8] We expended considerable effort in attempting to function Landahl's model[10,11] and were successful.[5] But we felt, even during this effort, that too many assumptions had been made and that more interesting and up-to-date models were available. Of particular interest is the one developed by Beeckmans.[13,14] Beeckmans has thoroughly considered the work of his predecessors, and his structure of the lung is based on Weibel's[15] description, which appears to be the most accurate available.[16]

Although Beeckmans' papers are quite descriptive of his model, there are significant details not available except in his program. Therefore, we initiated direct collaboration with Dr. Beeckmans as a consultant to the project. Before collaboration could begin, however, it was necessary to settle two questions. The first concerned the alteration of breathing mechanics in an individual subjected to a high-pressure helium-oxygen environment. The second concerned agreement upon generalized equations for the three physical mechanisms that the model considers, viz., sedimentation, diffusion, and impaction. The question of breathing mechanics was answered as a result of a personal conversation[16] with Commander N.R. Anthonisen, U.S. Naval Medical Center. Dr. Anthonisen has participated in studies of simulated

dives to 825 ft and reports that the flow rate, cycle time, and tidal volume are about the same in helium-oxygen mixtures as in air at ambient pressures. He expects that if there is a change, it would be in the direction of increased tidal volume and decreased cycle time. His findings justify the use of existing breathing patterns in our model.

The breathing patterns for which the model is being run are:

(1) Flow rate = 300 cm^3/sec
Cycle time = 4 sec
Tidal volume = 450 cm^3

(2) Flow rate = 300 cm^3/sec
Cycle time = 8 sec
Tidal volume = 900 cm^3

(3) Flow rate = 300 cm^3/sec
Cycle time = 12 sec
Tidal volume = 1350 cm^3

(4) Flow rate = 1000 cm^3/sec
Cycle time = 4 sec
Tidal volume = 1500 cm^3

Since these patterns are the ones classically run for air, our results may be directly compared with data at ambient conditions.

3.1 Modified Aerosol Deposition Equations

Impaction

The impaction equation which is used by both Landahl and Beeckmans is:

$$I = 150\ \rho\ d^2\ V/(R + 150\ \rho\ d^2\ V) \tag{4}$$

where: I = probability of inertial deposition

ρ = particle density

d = particle diameter

R = radius of airway

V = gas velocity

Hatch and Gross[12] indicate that Eqn. 4 may be arrived at by beginning with the following expression:

$$I = \frac{P_i}{1 + P_i} \tag{5}$$

where: P_i = impaction parameter

$$= \frac{vV}{gR}$$

where: g = gravitational acceleration

v = sedimentation velocity of particle

$$= \frac{\rho\ g\ d^2}{18\eta} \text{ (slip correction)}$$

where: η = gas viscosity

Combining:

$$P_i = \frac{\rho d^2 V}{18 \eta R} \text{ (slip correction)} \tag{6}$$

Therefore:

$$I = \frac{\frac{\rho d^2 V}{18\eta R} (s.c.)}{1 + \frac{\rho d^2 V}{18\eta R} (s.c.)}$$

Rewriting:

$$I = \frac{\rho d^2 V (s.c.)}{18 \eta} \Big/ \left(R + \frac{\rho d^2 V (s.c.)}{18\eta} \right) \tag{7}$$

Equation (7) may be used as a general expression for any gas and aerosol system. The value of the slip correction for our helium-oxygen atmosphere at the various pressures would, of course, be obtained from our previously tabulated numbers.[5] It may also be demonstrated that the relationship originally used by Landahl corresponds to our Equation (7). Comparing Equation (7) to Equation (4), the quantity 150 is seemingly equal to $\left(\frac{s.c.}{18\eta}\right)$. The term $(18\eta)^{-1}$ is approximately equal to 300 for air when η is expressed in units of poises. However, Landahl multiplied P_i by sin θ to account for the branching of the airways in the lung. Further, since Landahl uses $\theta = 30^\circ$ and sin $30^\circ = 0.5$, the coefficient in his equation is not 300 but 150. Therefore, to generalize Landahl's equation for any gas and branching angle, the factor 150 should be replaced by $\frac{\sin\theta\ (s.c.)}{18\eta}$.

Finally, it is concluded that Landahl's equation (Eqn. (4)) is based on firm grounds, and when expressed in general form, it becomes

$$I = \frac{\rho d^2 V \sin \theta \ (s.c.)}{18\eta} \Big/ \left(R + \frac{\rho d^2 V \sin \theta \ (s.c.)}{18\eta} \right) \tag{8}$$

or, if tabulated, values of v, which include the slip correction are to be used[5] the equation may be stated as

$$I = v V \sin \theta \Big/ \left(g R + v V \sin \theta \right) \tag{9}$$

Sedimentation

The equation used by Beeckmans[14] and his predecessors for deposition due to sedimentation is stated in final form as

$$S = 1 - \exp \left(- g d^2 \rho \tau \cos \psi' / 18\eta R \right) \ (s.c.) \tag{10}$$

where: S = probability of deposition due to sedimentation

τ = mean passage time of the particles

ψ' = angle of inclination of a tube with the horizontal

$\cos \psi'$ is commonly assigned a value of $2/\pi$.[11, 12, 13] This equation may be written more simply in terms of the sedimentation velocity and $\cos \psi'$ equals $2/\pi$.

$$S = 1 - \exp \left(- \frac{2 v \tau}{\pi R} \right) \tag{11}$$

By using Equation (11) one may directly substitute sedimentation data that has been previously tabulated[5] for the environment under consideration. These tabulations represent an improvement over simply calculated values inasmuch as they already

contain the slip correction factor, as well as corrected sedimentation equations for various ranges of Reynolds number. In fact, the simple Stokes sedimentation equation is used only up to a Reynolds number of 0.05. From 0.05 to 4 we have used Davies' equation,[17] and from 4 to 400 we have used Klyachko's equation.[18]

Diffusion

The equation used by Beeckmans[14] and his predecessors for diffusion is

$$D_i = 1 - \exp\left[(-7.31\, k\, T\, \tau / 6\pi\, R^2\, \eta\, d)\ (s.c.)\right] \qquad (12)$$

where: D_i = probability of deposition due to diffusion
k = Boltzmann's constant
T = absolute temperature

The coefficient of the exponential argument in this equation comes from Townsend's[19] solution of the problem of diffusion to perfectly absorbing walls having a circular cross-section. The dominant first term in his infinite series solution is 7.31. This equation was experimentally verified, and used by Beeckmans without further investigation. Equation (12) can be rewritten more simply in terms of the diffusion coefficient (D) and the slip correction:

$$D_i = 1 - \exp\ (-7.31\, D\tau / 2\, R^2) \qquad (13)$$

where: D = diffusion coefficient with slip correction

The slip-corrected diffusion coefficients for the atmosphere under investigation have previously been tabulated[5] and are therefore suitable for direct substitution into this equation and into the model.

3.2 Results

Calculations have been completed for the four breathing conditions of choice (see Introduction). These conditions are typified by the parameters of flow rate, cycle time, and tidal volume. In discussing each condition only the tidal volume will be referenced as that is the number which is different in each of the four cases. The results for the four conditions are tabulated in Tables 4 thru 7. It was found that the computer program would not function in the 0.001 micron size range for the 450 and 900 cm^2 tidal volume runs. A determination of the cause would have been most difficult and time consuming and it was felt that the trends were clearly indicated by data obtained for the other two tidal volumes. Through a small oversight data was not obtained in the 0.001 micron size range for $\rho = 2$ and $\rho = 3$ for the tidal volumes which were successfully run. Inasmuch as the curves have always been insensitive to the differences in density below about 0.1 micron as the physics of the situation would indicate, no further attempt was made to obtain this omitted data. For comparative purposes calculations have also been processed for air at 14.7 psia.

The results of all four runs have been plotted in Figures 14 thru 17. For purposes of clarity the total and lower tract deposition curves have been separated on the same page. Similarly, only the 10 and 500 psia lines have been plotted presenting the data as a series of envelopes within which the intervening values are found. The discussion of the results will be confined principally to the curves as presented in Figures 14 thru 17.

The most significant result apparent in this study is that the deposition curve for air lies within the 10 to 500 psia envelope in all cases with one or two minor

Table 4. Particle Retentions in the Total and Lower Respiratory Tract for He-O_2 (PO_2 = 160 mm Hg) at Various Pressures.

Flow Rate = 300 cm^3/sec
Cycle Time = 4 sec
Tidal Volume = 450 cm^3

d=0.001μ psia	ρ = 1 (air) Total	ρ = 1 (air) Lower	ρ = 1 Total	ρ = 1 Lower	ρ = 2 Total	ρ = 2 Lower	ρ = 3 Total	ρ = 3 Lower
10								
14.7								
20								
30								
40								
50								
100								
200								
300								
400								
500								
0.01μ								
10			0.7700	0.2420	0.7700	0.2420	0.7700	0.2420
14.7	0.7340	0.4282	0.7619	0.3079	0.7619	0.3079	0.7619	0.3079
20			0.7530	0.3605	0.7530	0.3605	0.7530	0.3605
30			0.7372	0.4197	0.7372	0.4197	0.7372	0.4197
40			0.7219	0.4532	0.7219	0.4532	0.7219	0.4532
50			0.7076	0.4730	0.7076	0.4730	0.7076	0.4730
100			0.6475	0.4990	0.6475	0.4990	0.6475	0.4990
200			0.5721	0.4780	0.5721	0.4780	0.5721	0.4780
300			0.5273	0.4535	0.5273	0.4535	0.5273	0.4535
400			0.4981	0.4348	0.4981	0.4348	0.4981	0.4348
500			0.4774	0.4206	0.4774	0.4206	0.4775	0.4206
0.1μ								
10			0.3259	0.4010	0.3300	0.3036	0.3341	0.3061
14.7	0.2402	0.2272	0.2934	0.2735	0.2972	0.2760	0.3008	0.2784
20			0.2696	0.2530	0.2729	0.2553	0.2763	0.2575
30			0.2425	0.2295	0.2454	0.2315	0.2483	0.2335
40			0.2266	0.2155	0.2293	0.2174	0.2320	0.2192
50			0.2165	0.2066	0.2190	0.2084	0.2215	0.2101
100			0.1939	0.1864	0.1960	0.1879	0.1980	0.1893
200			0.1814	0.1753	0.1833	0.1765	0.1852	0.1778
300			0.1774	0.1716	0.1793	0.1728	0.1811	0.1741
400			0.1753	0.1697	0.1771	0.1709	0.1789	0.1721
500			0.1740	0.1685	0.1758	0.1697	0.1775	0.1709
1.0μ								
10			0.3046	0.2465	0.3986	0.2996	0.4626	0.3300
14.7	0.2850	0.2305	0.2946	0.2386	0.3867	0.2907	0.4499	0.3210
20			0.2881	0.2334	0.3791	0.2849	0.4426	0.3157
30			0.2821	0.2286	0.3712	0.2789	0.4336	0.3091
40			0.2785	0.2257	0.3671	0.2757	0.4290	0.3057
50			0.2766	0.2242	0.3644	0.2736	0.4264	0.3037
100			0.2722	0.2206	0.3591	0.2695	0.4307	0.2994
200			0.2700	0.2188	0.3563	0.2673	0.4175	0.2970
300			0.2693	0.2183	0.3553	0.2665	0.4166	0.2964
400			0.2687	0.2177	0.3549	0.2662	0.4160	0.2959
500			0.2687	0.2177	0.3545	0.2659	0.4157	0.2957
10μ								
10			0.8483	0.0581	0.8857	0.0063	0.9087	0.0007
14.7	0.8503	0.0545	0.8480	0.0585	0.8854	0.0064	0.9084	0.0008
20			0.8479	0.0587	0.8852	0.0065	0.9082	0.0008
30			0.8477	0.0591	0.8850	0.0065	0.9080	0.0008
40			0.8476	0.0593	0.8849	0.0065	0.9079	0.0008
50			0.8476	0.0593	0.8849	0.0066	0.9078	0.0008
100			0.8474	0.0595	0.8847	0.0066	0.9077	0.0008
200			0.8473	0.0597	0.8846	0.0066	0.9076	0.0008
300			0.8473	0.0597	0.8846	0.0066	0.9076	0.0008
400			0.8473	0.0597	0.8846	0.0067	0.9076	0.0008
500			0.8473	0.0597	0.8846	0.0067	0.9075	0.0008

Table 5. Particle Retentions in the Total and Lower Respiratory Tract for He-O_2 (PO_2 = 160 mm Hg) at Various Pressures.

Flow Rate = 300 cm^3/sec
Cycle Time = 8 sec
Tidal Volume = 900 cm^3

d=0.001μ	ρ = 1 (air)		ρ = 1		ρ = 2		ρ = 3	
psia	Total	Lower	Total	Lower	Total	Lower	Total	Lower
10								
14.7								
20								
30								
40								
50								
100								
200								
300								
400								
500								
0.01μ								
10			0.8914	0.3218	0.8914	0.3218	0.8914	0.3217
14.7	0.8789	0.5711	0.8882	0.4093	0.8882	0.4093	0.8882	0.4093
20			0.8851	0.4794	0.8851	0.4794	0.8851	0.4794
30			0.8799	0.5593	0.8799	0.5593	0.8799	0.5593
40			0.8749	0.6069	0.8749	0.6069	0.8749	0.6069
50			0.8699	0.6374	0.8699	0.6374	0.8699	0.6374
100			0.8440	0.6987	0.8439	0.6986	0.8439	0.6986
200			0.7961	0.7057	0.7959	0.7056	0.7959	0.7056
300			0.7565	0.6867	0.7562	0.6864	0.7562	0.6864
400			0.7255	0.6664	0.7250	0.6658	0.7250	0.6658
500			0.7015	0.6488	0.7007	0.6480	0.7007	0.6480
0.1μ								
10			0.4910	0.4696	0.4928	0.4699	0.4982	0.4739
14.7	0.3772	0.3669	0.4455	0.4286	0.4457	0.4277	0.4504	0.4313
20			0.4127	0.3990	0.4117	0.3969	0.4160	0.4002
30			0.3764	0.3658	0.3740	0.3625	0.3776	0.3653
40			0.3554	0.3464	0.3523	0.3425	0.3555	0.3450
50			0.3418	0.3338	0.3382	0.3295	0.3412	0.3318
100			0.3106	0.3047	0.3061	0.2996	0.3086	0.3015
200			0.2925	0.2876	0.2876	0.2821	0.2899	0.2839
300			0.2863	0.2816	0.2813	0.2762	0.2836	0.2779
400			0.2831	0.2786	0.2781	0.2731	0.2802	0.2747
500			0.2811	0.2767	0.2761	0.2711	0.2783	0.2729
1.0μ								
10			0.4413	0.3909	0.5633	0.4752	0.6468	0.5275
14.7	0.4193	0.3720	0.4275	0.3791	0.5464	0.4612	0.6293	0.5138
20			0.4185	0.3713	0.5353	0.4520	0.6191	0.5056
30			0.4100	0.3639	0.5240	0.4425	0.6065	0.4953
40			0.4050	0.3595	0.5181	0.4375	0.6001	0.4901
50			0.4025	0.3573	0.5143	0.4343	0.5962	0.4869
100			0.3964	0.3520	0.5069	0.4279	0.5881	0.4801
200			0.3933	0.3492	0.5029	0.4245	0.5836	0.4764
300			0.3924	0.3484	0.5014	0.4233	0.5823	0.4753
400			0.3915	0.3477	0.5009	0.4228	0.5815	0.4746
500			0.3915	0.3477	0.5003	0.4223	0.5811	0.4743
10μ								
10			0.9353	0.0783	0.9554	0.0085	0.9686	0.0010
14.7	0.9367	0.0734	0.9352	0.0789	0.9552	0.0087	0.9684	0.0010
20			0.9351	0.0792	0.9551	0.0088	0.9683	0.0011
30			0.9349	0.0798	0.9550	0.0089	0.9682	0.0011
40			0.9348	0.0800	0.9550	0.0089	0.9681	0.0011
50			0.9348	0.0800	0.9549	0.0089	0.9681	0.0011
100			0.9348	0.0803	0.9548	0.0090	0.9680	0.0011
200			0.9347	0.0806	0.9548	0.0090	0.9680	0.0011
300			0.9347	0.0806	0.9548	0.0090	0.9680	0.0011
400			0.9347	0.0806	0.9548	0.0091	0.9680	0.0011
500			0.9347	0.0806	0.9548	0.0091	0.9680	0.0011

Table 6. Particle Retentions in the Total and Lower Respiratory Tract for He-O_2 (PO_2 = 160 mm Hg) at Various Pressures.

Flow Rate = 300 cm^3/sec
Cycle Time = 12 sec
Tidal Volume = 1350 cm^3

d=0.001μ	ρ = 1 (air)		ρ = 1		ρ = 2		ρ = 3	
psia	Total	Lower	Total	Lower	Total	Lower	Total	Lower
10			0.9850	0.0000				
14.7			0.9812	0.0000				
20			0.9776	0.0000				
30			0.9720	0.0000				
40			0.9676	0.0000				
50			0.9640	0.0000				
100			0.9536	0.0000				
200			0.9452	0.0034				
300			0.9412	0.0212				
400			0.9387	0.0528				
500			0.9389	0.0915				
0.01μ								
10			0.9303	0.3490	0.9303	0.3490	0.9303	0.3490
14.7	0.9228	0.6196	0.9281	0.4440	0.9281	0.4440	0.9281	0.4440
20			0.9262	0.5200	0.9262	0.5200	0.9262	0.5200
30			0.9233	0.6068	0.9234	0.6067	0.9234	0.6067
40			0.9208	0.6588	0.9208	0.6586	0.9208	0.6586
50			0.9184	0.6923	0.9184	0.6923	0.9184	0.6923
100			0.9059	0.7656	0.9059	0.7656	0.9059	0.7656
200			0.8797	0.7926	0.8799	0.7928	0.8799	0.7928
300			0.8643	0.7873	0.8655	0.7884	0.8655	0.7884
400			0.8320	0.7754	0.8345	0.7778	0.8345	0.7778
500			0.8133	0.7630	0.8170	0.7668	0.8171	0.7668
0.1μ								
10			0.6038	0.5836	0.6395	0.6181	0.6445	0.6218
14.7	0.4619	0.4518	0.5490	0.5331	0.5938	0.5770	0.5983	0.5805
20			0.5077	0.4948	0.5596	0.5459	0.5638	0.5491
30			0.4604	0.4503	0.5204	0.5097	0.5241	0.5126
40			0.4324	0.4239	0.4970	0.4879	0.5003	0.4906
50			0.4141	0.4065	0.4814	0.4733	0.4846	0.4759
100			0.3719	0.3663	0.4443	0.4382	0.4471	0.4405
200			0.3475	0.3428	0.4216	0.4165	0.4242	0.4181
300			0.3392	0.3348	0.4136	0.4088	0.4162	0.4109
400			0.3348	0.3306	0.4094	0.4047	0.4119	0.4068
500			0.3321	0.3280	0.4067	0.4021	0.4093	0.4042
1.0μ								
10			0.5342	0.4873	0.6958	0.6147	0.7682	0.6575
14.7	0.5068	0.4627	0.5171	0.4720	0.6800	0.6018	0.7531	0.6462
20			0.5058	0.4618	0.6695	0.5931	0.7440	0.6393
30			0.4950	0.4521	0.6587	0.5840	0.7328	0.6305
40			0.4886	0.4463	0.6530	0.5792	0.7270	0.6259
50			0.4854	0.4433	0.6493	0.5761	0.7235	0.6231
100			0.4776	0.4363	0.6420	0.5699	0.7161	0.6171
200			0.4735	0.4325	0.6381	0.5666	0.7119	0.6137
300			0.4724	0.4315	0.6367	0.5654	0.7108	0.6128
400			0.4712	0.4303	0.6362	0.5649	0.7100	0.6121
500			0.4712	0.4304	0.6356	0.5644	0.7096	0.6118
10μ								
10			0.9626	0.0858	0.9759	0.0094	0.9827	0.0011
14.7	0.9636	0.0803	0.9625	0.0864	0.9758	0.0096	0.9826	0.0011
20			0.9624	0.0867	0.9757	0.0097	0.9826	0.0012
30			0.9623	0.0874	0.9756	0.0098	0.9825	0.0012
40			0.9622	0.0877	0.9756	0.0098	0.9824	0.0012
50			0.9622	0.0877	0.9756	0.0098	0.9824	0.0012
100			0.9622	0.0880	0.9755	0.0099	0.9824	0.0012
200			0.9621	0.0884	0.9755	0.0099	0.9824	0.0012
300			0.9621	0.0884	0.9755	0.0099	0.9824	0.0012
400			0.9621	0.0884	0.9755	0.0100	0.9824	0.0012
500			0.9621	0.0884	0.9755	0.0100	0.9823	0.0012

Table 7. Particle Retentions in the Total and Lower Respiratory Tract for He-O_2 (PO_2 = 160 mm Hg) at Various Pressures.

Flow Rate = 1000 cm^3/sec
Cycle Time = 4 sec
Tidal Volume = 1500 cm^3

d=0.001μ	ρ = 1 (air)		ρ = 1		ρ = 2		ρ = 3	
psia	Total	Lower	Total	Lower	Total	Lower	Total	Lower
10			0.9726	0.0000				
14.7			0.9680	0.0000				
20			0.9639	0.0000				
30			0.9589	0.0000				
40			0.9556	0.0003				
50			0.9532	0.0014				
100			0.9469	0.0329				
200			0.9419	0.1662				
300			0.9392	0.2874				
400			0.9374	0.3780				
500			0.9360	0.4457				
0.01μ								
10			0.9297	0.6661	0.9297	0.6661	0.9297	0.6660
14.7	0.9139	0.7885	0.9266	0.7159	0.9266	0.7158	0.9266	0.7158
20			0.9229	0.7303	0.9229	0.7502	0.9229	0.7502
30			0.9155	0.7841	0.9155	0.7841	0.9155	0.7841
40			0.9074	0.8004	0.9074	0.8004	0.9074	0.8004
50			0.8989	0.8079	0.8989	0.8079	0.8989	0.8079
100			0.8514	0.7975	0.8514	0.7975	0.8514	0.7975
200			0.7703	0.7380	0.7704	0.7380	0.7704	0.7380
300			0.7184	0.6938	0.7184	0.6938	0.7184	0.6938
400			0.6847	0.6641	0.6847	0.6641	0.6847	0.6641
500			0.6615	0.6434	0.6615	0.6434	0.6615	0.6434
0.1μ								
10			0.5095	0.5021	0.5129	0.5044	0.5163	0.5067
14.7	0.4173	0.4133	0.4779	0.4720	0.4811	0.4741	0.4842	0.4763
20			0.4524	0.4474	0.4555	0.4495	0.4585	0.4516
30			0.4189	0.4149	0.4220	0.4170		
40			0.3959	0.3924	0.3989	0.3944		
50			0.3791	0.3759	0.3822	0.3781		
100			0.3347	0.3320	0.3379	0.3343		
200			0.3056	0.3032	0.3088	0.3055		
300			0.2953	0.2930	0.2984	0.2952		
400			0.2898	0.2875	0.2929	0.2828		
500			0.2863	0.2841	0.2895	0.2864		
1.0μ								
10			0.4759	0.3945	0.6021	0.4609	0.6599	0.4670
14.7	0.4532	0.3715	0.4633	0.3817	0.5912	0.4494	0.6485	0.4549
20			0.4548	0.3729	0.5839	0.4418	0.6419	0.4478
30			0.4464	0.3643	0.5763	0.4339	0.6339	0.4391
40			0.4414	0.3592	0.5724	0.4297	0.6298	0.4346
50			0.4387	0.3564	0.5698	0.4269	0.6274	0.4320
100			0.4326	0.3500	0.5646	0.4214	0.6222	0.4263
200			0.4292	0.3466	0.5618	0.4184	0.6193	0.4232
300			0.4282	0.3456	0.5608	0.4173	0.6185	0.4223
400			0.4273	0.3446	0.5604	0.4169	0.6180	0.4217
500			0.4273	0.3446	0.5600	0.4165	0.6178	0.4214
10μ								
10			0.9617	0.0145	0.9727	0.0005	0.9791	0.0000
14.7	0.9621	0.0142	0.9617	0.0145	0.9726	0.0005	0.9790	0.0000
20			0.9616	0.0146	0.9726	0.0005	0.9790	0.0000
30			0.9616	0.0146	0.9725	0.0005	0.9790	0.0000
40			0.9616	0.0146	0.9725	0.0005	0.9790	0.0000
50			0.9616	0.0146	0.9725	0.0005	0.9789	0.0000
100			0.9616	0.0146	0.9725	0.0006	0.9789	0.0000
200			0.9615	0.0146	0.9725	0.0005	0.9789	0.0000
300			0.9615	0.0146	0.9725	0.0005	0.9789	0.0000
400			0.9615	0.0146	0.9725	0.0005	0.9789	0.0000
500			0.9615	0.0146	0.9725	0.0005	0.9789	0.0000

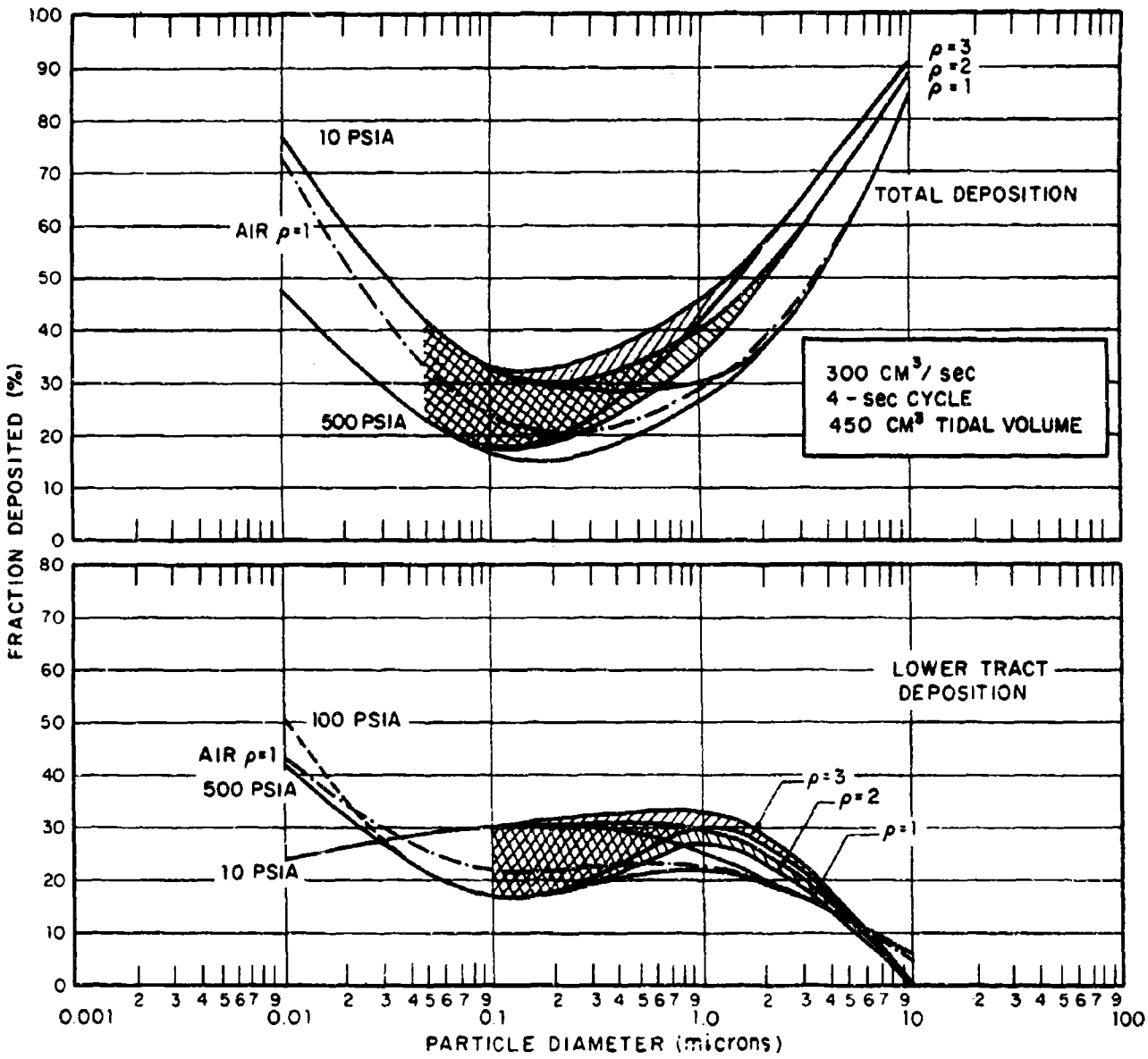

Figure 14. Total and Lower Respiratory Tract Deposition. He-O_2 (PO_2 = 160 mm Hg) at Various Pressures.

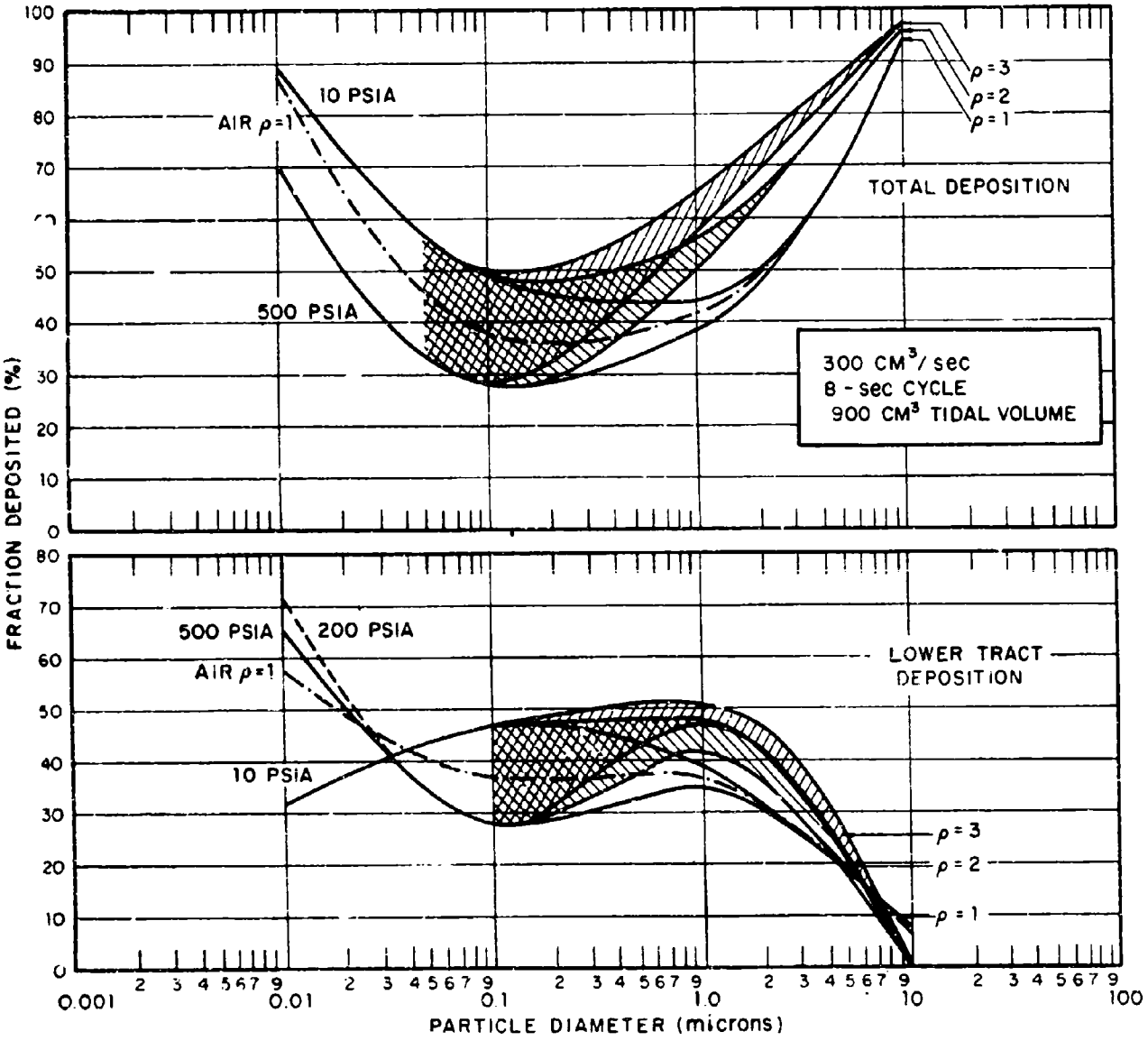

Figure 15. Total and Lower Respiratory Tract Deposition. He-O_2 (PO_2 = 160 mm Hg) at Various Pressures.

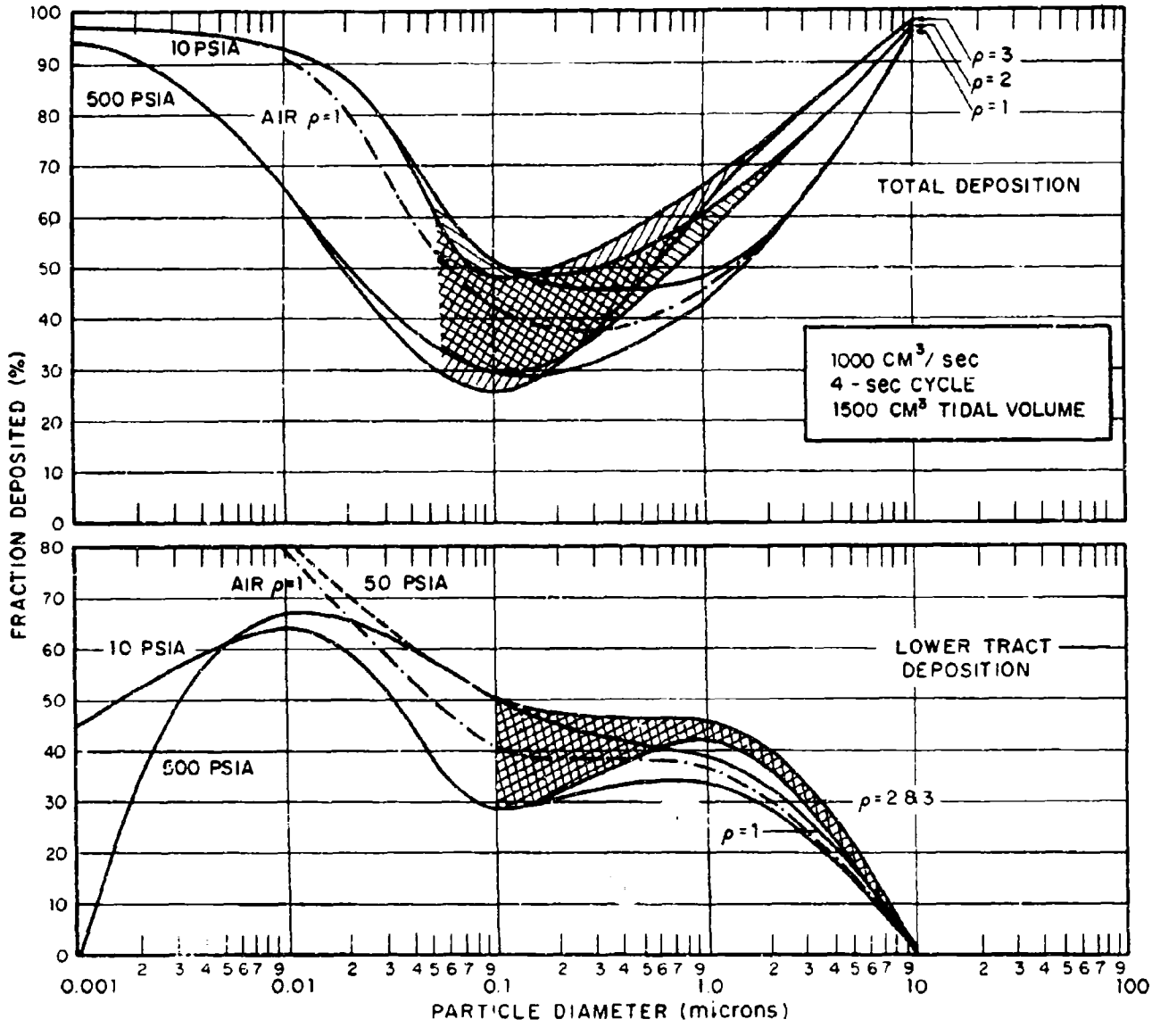

Figure 16. Total and Lower Respiratory Tract Deposition. He-O_2 (PO_2 = 160 mm Hg) at Various Pressures.

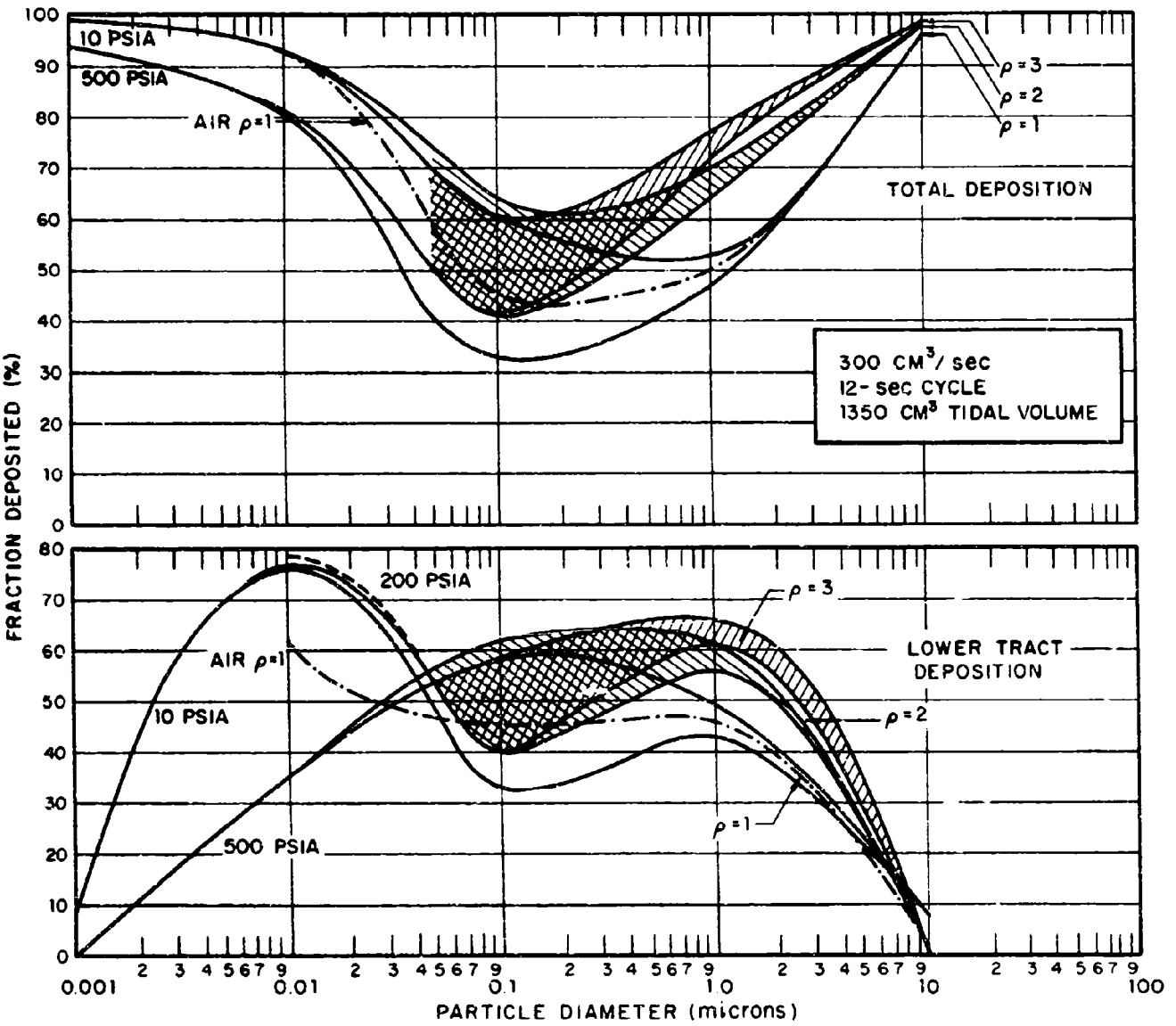

Figure 17. Total and Lower Respiratory Tract Deposition. He-O_2 (PO_2 = 160 mm Hg) at Various Pressures.

exceptions. Lower tract deposition increases with increasing pressure and at the highest pressures is significantly greater than in air. Conversely total deposition decreases with increasing pressure and has its lowest values at the highest pressures. Differences from the values found in air for both total and lower tract depositions are practically non-existent for particle diameters greater than 1 micron in all cases. The only observable difference in deposition about 1 micron is due to plotted density variations within each breathing pattern. Also the envelopes are noted to be quite narrow above 1 micron. Below approximately 0.1 micron and definitely below 0.04 micron there are no observable differences due to density in any of the breathing patterns. Deposition apparently decreases even in the lower tract (as it does in the total case) with increasing pressure below 0.04 microns.

The general shape of all curves roughly corresponds to the shape of the air deposition curves. The most notable variances being in those cases where data for 0.001 micron diameter particles have been obtained and for the 1350 cm^2 tidal volume. The greatest increases in deposition over the values found for air are at the 0.01 micron case for all breathing patterns. Because particle density is of no consideration below 0.01 micron it may simply be stated that for all breathing patterns the increase in the lower tract deposition is 20% or less due to changes in pressure. This finding is significant in that the increase is notable when depositions are running no less than 20% for any pressure and any breathing pattern.

3.2 General Conclusions

Appreciating the limitations on both studies reported herein, several general conclusions may now be attempted regarding the direct relationship of this work to the deep submergence environment. Particles are produced from heated surfaces within the high pressure environment. Their size is modestly effected by increasing pressure and is in the submicron range. Increasing pressure dramatically reduces the numbers of particles produced. There are definite increases in lower pulmonary deposition due to the increase in pressure and overall size ranges and breathing patterns. These increases are substantial but not overwhelming. If computer models of lungs may be considered adequate, and if only this one particle source is present, then the net hazard from this source of particulates is apparently reduced with increasing pressure and rudimentary control methods may be applied. Of course, our previous work on the possibilities of electrostatic precipitation in the high pressure environment[5] and our current efforts in filtration seem to indicate that reduced efficiencies are to be expected at the highest pressures, then the picture may change somewhat, but hopefully reduce to no worse a problem than is currently encountered in ambient pressure environments.

While the preceding comments may certainly be looked upon as favorable and indicative of nominal or reduced human risk due to aerosols, strong cautions must be observed regarding the lack of data on other sources of particulates, especially those which might be found in the larger size range above 0.1 micron. However, even these larger sizes whose collection efficiency within the lung is very high, differ almost not at all in their deposition patterns from conditions in air.

Our final conclusion to be stated in this report is based upon all our previous work, investigations, and conversations, and that is, to re-emphasize the strong need for actual samples from an inhabited high-pressure environment. It is hoped that the results of such samples will only confirm our positive findings indicating low risk, but without the confirmatory data, extreme caution is warranted in applying this work.

LITERATURE CITED

1. Polydorova, M.: The Preparation and Properties of a Tungsten Oxide Aerosol. Staub, V. 25, #12, p. 16-18, English Translation, (Dec 1965).

2. Binek, Bedrich: Sampling Finely Dispersed Aerosols for Electron-Microscopic Particle Analysis. Staub, V. 25, #7, p. 13-19, English Translation, (July 1965).

3. Maiwald, E.: A Tungsten Oxide Test Aerosol. Staub, V. 25, #12, p. 13-15, English Translation. (Dec, 1965).

4. Goldsmith, P., F.G. May and R.D. Wiffen: Chromium Trioxide Aerosol from Heated 80:20 Nickel-Chromium Wire. Nature 210, p. 475-477 (Apr. 30, 1966).

5. Gussman, Robert A.: Aerosol Behavior in High Pressure Environments. Performed under Contract No. N00014-68-C-0271, Department of the Navy, Washington, D.C., Bolt Beranek and Newman Inc., Cambridge, Mass. (28 Feb. 1968).

6. Corn, Morton: Statistical Reliability of Particle Size Distributions Determined by Microscopic Techniques. AIHA J., V. 26, #1, p. 8-16 (Jan-Feb. 1965)

7. Drinker, P. and T. Hatch: Industrial Dust, McGraw-Hill Book Co., Inc., New York, 1954.

8. International Radiological Protection Commission: Deposition and Retention Models for Internal Dosimetry of the Human Respiratory Tract. Health Physics, Vol. 12, #1, p. 173-207, Pergamon Press, 1966.

9. Findeisen, W.: The Deposition of Small Airborne Particles in the Human Lung During Respiration. Arch. Ges. Physiol. p. 236-367 (1935).

10. Landahl, H.D.: On The Removal of Air-Borne Droplets by the Human Respiratory Tract: 1. The Lung. Bull. of Mathematical Biophysics, Vol. 12, p. 43 (1950).

11. Landahl, H.D.: Particle Removal by the Respiratory System-Note on the Removal of Airborne Particulates by the Human Respiratory Tract with Particular Reference to the Role of Diffusion. Bull. of Mathematical Biophysics, Vol. 25 (1963).

12. Hatch, T.F. and P. Gross: Pulmonary Deposition and Retention of Inhaled Aerosols. Academic Press, New York, 1964.

LITERATURE CITED - con't.

13. Beeckmans, J.M.: The Deposition of Aerosols in the Respiratory Tract. 1. Mathematical Analysis & Comparison with Experimental Data. Canadian J. of Physiology & Pharmacology, Vol. 43, p. 157 (1965).

14. Beeckmans, J.M.: Correction Factor for Size-Selective Sampling Results, Based on a New Computed Alveolar Deposition Curve. Ann. Occup. Hyg., Vol. 8, p. 221-231, Pergamon Press (1965).

15. Weibel, E.R.: Morphometry of the Human Lung. Academic Press, New York, 1963.

16. Anthonisen, N.R., Cdr., U.S. Naval Medical Corp., Mar. 1969.

17. Davies, C.N.: Definitive Equations for the Fluid Resistance of Spheres. The Proceedings of the Physical Society, Vol. 57, Pt. 4, #322 (1 July 1945).

18. Fuchs, N.A.: The Mechanics of Aerosols. The MacMillian Co., New York, 1964.

19. Townsend, J.S.: The Diffusion of Ions into Gases. Trans. Roy. Soc., 193A, p. 125-158 (1900).

APPENDIX I: SYMBOLS

This list of symbols pertains to the project as a whole and not simply to this report. Therefore, symbols may be listed herein which are not used in this specific report.

A = a numerical factor having a value of approximately unity

A_o = first Cunningham correction coefficient = 1.257

B = second Cunningham correction coefficient = 0.400, mobility of the aerosol particles

C = third Cunningham correction coefficient = 1.10, in filtration, a numerical factor of 0.5 to 0.75

C_D = drag coefficient

D = diffusion coefficient

D_i = probability of deposition due to diffusion

E = collecting field strength, efficiency of intact filter, voltage

E_D = diffusional filtration efficiency

E_G = gravitational filtration efficiency

E_I = inertial filtration efficiency

E_j = filtration efficiency due to all mechanisms (j = ERIGM Qq)

E_M = molecular filtration efficiency

E_o = charging field strength

E_{Qq} = electrostatic filtration efficiency (Also: E_{oq}, only fiber is charged; E_{Qo}, only aerosol is charged.)

E_R = direct interception filtration efficiency

$E\beta_j$ = E_j and includes consideration of the interference effect

F = drag on particle

I = current, probability of inertial deposition

I_d = collision intergral

K = agglomeration coefficient

$K_{1,2,3}$ = thermal conductivity

M = collection efficiency, molecular weight

N_D = gravational filtration parameter

N_I = inertial filtration parameter

N_M = molecular filtration parameter

N_o = ion concentration

N_{Qq} = electrostatic filtration parameter

N_R = direct interception filtration parameter

P = pressure in atmospheres

P_c = critical pressure

P_e = Peclet number

P_i = impaction parameter

P_{pc} = psuedo critical pressure

R = radius, gas constant

R_1 = radius of discharge electrode

R_2 = radius of collecting electrode

R_e = Reynolds number

S = ratio of particulate sphere of influence to particle radius, saturation, probability of deposition due to sedimentation

Stk. = Stokes number

T = absolute temperature

T_c = critical temperature

T_d = droplet temperature

T_{pc} = pusedo critical temperature

U_o = velocity of particle (re: mobility, B)

V = gas velocity

V' = applied potential

V_L = molecular volume

Y = mole fraction

Z = electric mobility of ions

Z_2 = electric mobility of O_2 ions

Z_3 = electric mobility of He ions

Z_r = reduced electric mobility of ions

$\bar{c}$ = R.M.S. velocity

d = particle diameter (in filtration as d_p)

d_f = fiber diameter

e = electronic charge

f = fraction

g = gravitational acceleration

h = height

i = current per unit length of electrode

k = Boltzmann's constant

m = ion mass, droplet mass

n = number concentration of particles, number of electronic charges, e

n_o = initial number concentration of particles

n_s = saturation charge

p = a factor (re: electrification), droplet vapor pressure

p_t = liquid vapor pressure

q = charge acquired in time, t

r = radial distance from electrode centerline

r_{12} = collision diameter

s = fraction of molecules reflected diffusely

t = time

u = drift velocity of particles

v = sedimentation velocity

α = evaporation (condensation) coefficient

β = f(s) (re: slip correction), volume fraction of fibers

γ = 0.499 as extracted from the current expression for λ, surface tension

Δ = vapor shell thickness

δ = 1 for specular reflections of the molecule from a particle but generally $\delta = (1 + \pi s/8)$ (re: slip correction), saturation

ϵ = dielectric constant

ϵ_o = dielectric constant of a vacuum. 8.85434×10^{6} amp-sec/volt-cm

η = viscosity of the fluid medium

θ = integer

λ = mean free path of gas molecules

μ = micron

$\nu = (RT/2\pi M)$

ρ = particulate density

ρ_L = liquid density

ρ' = gas density

τ = relaxation time, mean passage time of particles

$\chi = \frac{2\lambda}{d}$, the Knudsen number

ψ' = angle of inclination of a tube with the horizontal

Unclassified

Security Classification

DOCUMENT CONTROL DATA - R & D

Security classification of title, body of abstract and indexing annotation must be entered when the overall report is classified)

1 ORIGINATING ACTIVITY (Corporate author) Bolt Beranek and Newman Inc. 50 Moulton Street Cambridge, Massachusetts	2a. REPORT SECURITY CLASSIFICATION Unclassified 2b. GROUP

3 REPORT TITLE

AEROSOL BEHAVIOR IN HIGH PRESSURE ENVIRONMENTS

4 DESCRIPTIVE NOTES (Type of report and, inclusive dates)

Special Period Covered: 1 March - 31 October 1969

5 AUTHOR(S) (First name, middle initial, last name)

Robert A. Cussman
Anthony M. Sacco

6 REPORT DATE	7a. TOTAL NO OF PAGES	7b. NO OF REFS
30 October 1969	55	19

8a. CONTRACT OR GRANT NO	9a. ORIGINATOR'S REPORT NUMBER(S)
N00014-69-C-0228 b. PROJECT NO NR 303-829 c. d	9b. OTHER REPORT NO(S) (Any other numbers that may be assigned this report)

10 DISTRIBUTION STATEMENT

This document has been approved for public release and sale. Its distribution is unlimited.

11 SUPPLEMENTARY NOTES	12 SPONSORING MILITARY ACTIVITY
TECH, OTHER	Department of the Navy Office of Naval Research Washington, D.C. 20360

13 ABSTRACT

This report finalizes two phases of a broad study whose general purpose is to elucidate hazards to personnel arising from aerosols in high pressure helium-oxygen atmospheres. Studies have been completed on the generation of aerosols within high pressure environments and experimental evidence has been gathered which generally indicates that particle diameter increases with increasing pressure to a slight degree but there is a remarkable reduction in numbers concentration of particles. Pulmonary deposition models have been finalized and indicate increases in deposition in the lower respiratory tract with increasing pressure.

DD FORM 1 NOV 65 1473 (PAGE 1)

S/N 0101-807-6811

Unclassified

Security Classification

14 KEY WORDS	LINK A		LINK B		LINK C	
	ROLE	WT	ROLE	WT	ROLE	WT
Aerosol aerosol formation pulmonary deposition aerosol mechanics deep submergence						